J|A|C|S ARTICLES

Published on Web 04/22/2009

# Theoretical and Experimental Studies of the Conversion of Chromopyrrolic Acid to an Antitumor Derivative by Cytochrome P450 StaP: The Catalytic Role of Water Molecules

Yong Wang,[†] Hui Chen,[†] Masatomo Makino,[‡] Yoshitsugu Shiro,[‡] Shingo Nagano,*[,‡] Shumpei Asamizu,[§,||] Hiroyasu Onaka,*[,§,||] and Sason Shaik*[,†]

*The Institute of Chemistry and the Lise Meitner-Minerva Center for Computational Quantum Chemistry, Hebrew University of Jerusalem, Givat Ram Campus, 91904 Jerusalem, Israel, Biometal Science Laboratory, RIKEN SPring-8 Center, Hyogo 679-5148, Japan, and Department of Biotechnology, Faculty of Engineering, and Biotechnology Research Center, Toyama Prefectural University, Toyama 939-0398, Japan*

Received January 17, 2009; E-mail: sason@yfaat.ch.huji.ac.il

***Abstract:*** Chromopyrrolic acid (CPA) oxidation by cytochrome P450 StaP is a key process in the biosynthesis of antitumor drugs (Onaka, H.; Taniguchi, S.; Igarashi, Y.; Furumai, T. *Biosci. Biotechnol. Biochem.* **2003**, *67*, 127−138), which proceeds by an unusual C−C bond coupling. Additionally, because CPA is immobilized by a hydrogen-bonding array, it is prohibited from undergoing direct reaction with Compound I, the active species of P450. As such, the mechanism of P450 StaP poses a puzzle. In the present Article, we resolve this puzzle by combination of theory, using QM/MM calculations, and experiment, using crystallography and reactivity studies. Theory shows that the hydrogen-bonding machinery of the pocket deprotonates the carboxylic acid groups of CPA, while the nearby $His_{250}$ residue and the crystal waters, $Wat_{644}$ and $Wat_{789}$, assist the doubly deprotonated CPA to transfer electron density to Compound I; hence, CPA is activated toward proton-coupled electron transfer that sets the entire mechanism in motion. The ensuing mechanism involves a step of C−C bond formation coupled to a second electron transfer, four proton-transfer and tautomerization steps, and four steps where $Wat_{644}$ and $Wat_{789}$ move about and mediate these events. Experiments with the dichlorinated substrate, CCA, which expels $Wat_{644}$, show that the enzyme loses its activity. H250A and H250F mutations of P450 StaP show that $His_{250}$ is important, but in its absence $Wat_{644}$ and $Wat_{789}$ form a hydrogen-bonding diad that mediates the transformation. Thus, *the water diad emerges as the minimal requisite element that endows StaP with function.* This highlights the role of water molecules as biological catalysts that transform a P450 to a peroxidase-type (Derat, E.; Shaik, S. *J. Am. Chem. Soc.* **2006**, *128*, 13940−13949).

## Introduction

The ubiquitous cytochrome P450 enzymes (P450s), which are widely distributed in plants, bacteria, insects, mammals, etc., are considered to be very important catalytic heme-containing proteins, due to their vital roles in the metabolism of drugs and in the biosynthesis of critical endogenous chemical compounds such as hormones.[1] These enzymes use dioxygen, two reducing equivalents, and two protons to generate an active species, so-called Compound I (Cpd I), **1** in Scheme 1, which has three unpaired electrons, two in $\pi^*$ orbitals of the iron-oxo moiety and one in the $a_{2u}$ orbital of the porphyrin cation radical ($Por^{+\bullet}$). As such, the total oxidation state of Cpd I is +5, two oxidation-equivalents above the resting state and the ferric product complex of the oxidized substrates.

***Scheme 1.*** Cpd I Species: **1** in P450, **2** in HRP, and **3** in C*c*P[a]

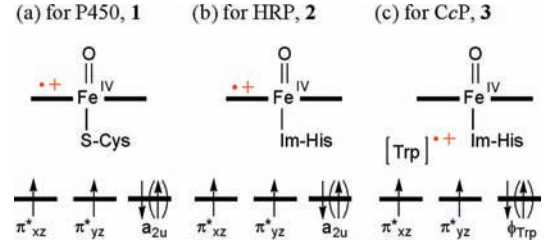


[a] The arrows in the three singly occupied orbitals represent the spin-up and/or spin-down electrons. The spin-down in the third orbital creates a doublet state ($S = 1/2$), and the spin-up (in parentheses) creates a quartet state ($S = 3/2$).

It is commonly accepted that Cpd I, **1**, is the active oxidant of P450s,[1,2] which can catalyze a wide variety of chemical transformations including hydroxylation of inert C−H bonds, epoxidation of C=C bonds, dealkylations, etc. In all of these processes, Cpd I inserts an [O] atom into a variety of bonds in reaction mechanisms, which involve radical intermediates, for example, by initial hydrogen abstraction from an alkane, or a radical attack on the double bond, etc. Cpd I is known also in

[†] Hebrew University of Jerusalem.
[‡] RIKEN SPring-8 Center.
[§] Department of Biotechnology, Toyama Prefectural University.
[||] Biotechnology Research Center, Toyama Prefectural University.

(1) (a) Ortiz de Montellano, P. R. *Cytochrome P450: Structure, Mechanism and Biochemistry*, 3rd ed.; Kluwer Academic/Plenum: New York, 2005. (b) Sigel, A., Sigel, H., Sigel, R. K. O., Eds. Ubiquitous Roles of Cytochrome P450 Proteins. *Metal Ions in Life Science*; John Wiley & Sons Ltd.: West Sussex, U.K., 2007; Vol. 3.


10.1021/ja9003365 CCC: $40.75 

***Scheme 2.*** (a) Formation of Staurosporine (STA) from L-Tryptophan via Chromopyrrolic Acid (CPA); and (b) Analogous Transformation of CCA to Rebeccamycin[a]

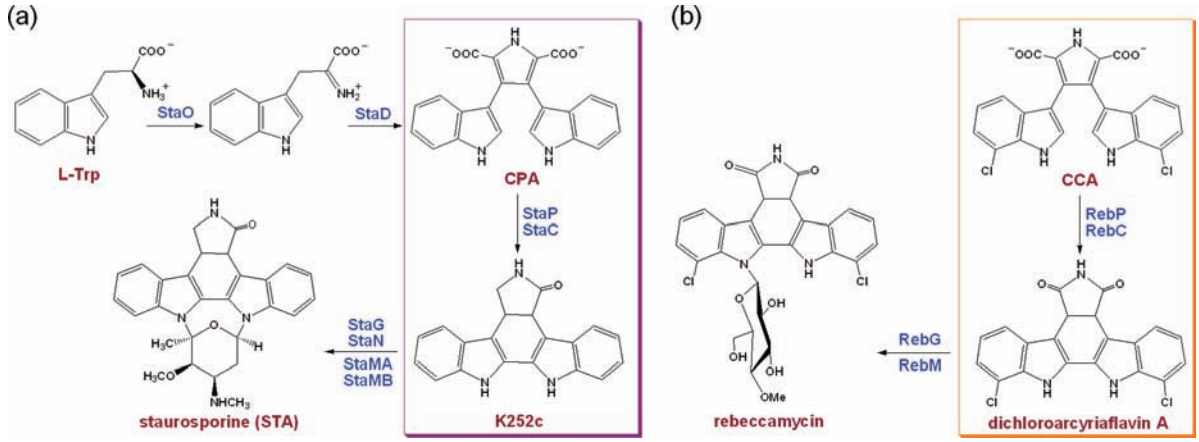


[a] Shorthand notations of the enzymes involved are indicated above the arrows. The aryl−aryl coupling induced by the P450s is framed.

peroxidases where it oxidizes substrates by electron-transfer or proton-coupled electron-transfer (PCET) mechanisms,[3] as the one transpiring when horseradish peroxidase (HRP) oxidizes ferulic acid and phenols in general.[4] The Cpd I species of peroxidases contains an imidazole ligand from a histidine residue, **2** in Scheme 1, and is hence a much better electron acceptor than the corresponding Cpd I of P450s, **1**, in which the proximal ligand is a thiolate of cysteine.[5] So much so, that in one member of the peroxidases, Cytochrome *c* Peroxidase (C*c*P), the Cpd I species oxidizes a Trp residue of the protein[6] and forms the one electron reduced Cpd II species (possibly protonated), **3** in Scheme 1, that performs the oxidation of Cytochrome *c* by electron abstraction. Indeed, the powerful electron-accepting ability of Cpd I species makes these complexes *"electronic chameleons"*, very susceptible to the environment, and hence capable of adopting their electronic properties and structures to the environments that accommodate them.[5a] Nevertheless, because P450 Cpd I is a much lesser electron acceptor than peroxidase Cpd I,[5c] one might have thought that it is safe to assume that P450 Cpd I will conserve its structure in **1** with small modifications due to the modulation of the electron donation from the thiolate ligand to the porphyrin cation radical moiety.[7] However, this assumption breaks down with Cpd I of P450 StaP (CYP 245A1), which has been shown recently to adopt an electronic structure closer to Cpd II, and to perform a peroxidase-like activity.[8] It is this intriguing activity that forms the focus of the present Article, which involves interplay of theoretical QM/MM calculations, site-directed mutagenesis, and X-ray crystallography, designed to elucidate the mechanism of action of P450 StaP Cpd I. Let us start with the story of this enzyme and its indolocarbazole biosynthesis where P450 StaP is involved.

Indolocarbazoles, such as staurosporine (STA) and rebeccamycin, shown in Scheme 2, are a family of natural alkaloids that are isolated from several microorganisms.[9] These natural products have attracted much attention because of their strong inhibitory activity on protein kinase or DNA topoisomerase I, which makes them therapeutically important anticancer agents. STA is biosynthesized by the following reactions indicated in Scheme 2a. Two IPA imines derived from tryptophan are coupled by the enzyme StaD to form chromopyrrolic acid (CPA). Next, P450 StaP catalyzes the conversion of CPA into a six-ring indolocarbazole scaffold, so-called K252c, which undergoes N-glycosylation and methylation by a series of enzymes to produce the final product STA.[10] A related transformation is the aryl−aryl coupling of dichlorochromopyrrolic acid (CCA), a dichlorinated CPA, which occurs en route to the formation of rebeccamycin (Scheme 2b). This process is catalyzed by P450 RebP,[11] which is homologous to P450 StaP, and will be examined here experimentally using P450 StaP.

There is a recent surge of interest in P450 StaP, not only because of the importance of staurosporine, but also because of the unusual transformation induced by this enzyme involving overall: C−C coupling, loss of two H atoms, and an oxidative decarboxylation (Scheme 2). Initial mechanistic studies by Howard-Jones and Walsh[10a] have shown that the carboxylic acid groups in CPA are necessary because the reaction does not take place in their absence. Further investigations have led to two alternative hypotheses, which are depicted in Scheme 3.

Thus, Howard-Jones and Walsh[12] postulated that the reaction proceeds via the common Cpd I species (**1**, Scheme 1) and provided evidence suggesting that the enzyme catalyzes first the C−C bond formation, by double hydrogen atom transfer (2HT), followed by a series of nonenzymatic reactions to

(2) (a) Makris, T. M.; Denisov, I.; Schlichting, I.; Sligar, S. G. Activation of molecular oxygen by cytochrome P450. In *Cytochrome P450: Structure, Mechanism and Biochemistry*, 3rd ed.; Ortiz de Montellano, P. R., Ed.; Kluwer Academic/Plenum Publishers: New York, 2005; pp 149−182. (b) Sono, M.; Roach, M. P.; Coulter, E. D.; Dawson, J. H. *Chem. Rev.* **1996**, *96*, 2841–2887. (c) Groves, J. T. Models and mechanisms of cytochrome P450 action. In *Cytochrome P450: Structure, Mechanism, and Biochemistry*; Ortiz de Montellano, P. R., Ed.; Kluwer Academic/Plenum Publishers: New York, 2005; pp 1−43.

(3) (a) Poulos, T. L. *Nat. Prod. Rep.* **2007**, *24*, 504–510. (b) Poulos, T. L. In *The Porphyrin Handbook*; Kadish, K. M., Smith, K. M., Guilard, R., Eds.; Academic Press: New York, 2000; Vol. 4, pp 189−218. (c) Colas, C.; Ortiz de Montellano, P. R. *Chem. Rev.* **2003**, *103*, 2305–2332. (d) Dunford, H. B. *Heme Peroxidases*; Wiley-VCH: New York, 1999.

(4) Derat, E.; Shaik, S. *J. Am. Chem. Soc.* **2006**, *128*, 13940–13949.

(5) (a) de Visser, S. P.; Shaik, S.; Sharma, P. K.; Kumar, D.; Thiel, W. *J. Am. Chem. Soc.* **2003**, *125*, 15779–15788. (b) Ogliaro, F.; de Visser, S. P.; Shaik, S. *J. Inorg. Biochem.* **2002**, *91*, 554–567. (c) See in particular the analysis of the orbital and field effect contributions to the poorer electron affinity with a thiolate ligand (as in P450) as compared to a histidine ligand (as in HRP) in: Ogliaro, F.; de Visser, S. P.; Shaik, S. *J. Inorg. Biochem.* **2002**, *91*, 554–567. (d) de Visser, S. P.; Shaik, S.; Sharma, P. K.; Kumar, D.; Thiel, W. *J. Am. Chem. Soc.* **2003**, *125*, 15779–15788.

(6) Barrows, T. P.; Bhaskar, B.; Poulos, T. L. *Biochemistry* **2004**, *43*, 8826–8834.

***Scheme 3.*** Mechanistic Proposals for C−C Coupling in CPA by StaP (a) via Initial Dual Hydrogen Atom Transfer (2HT), and (b) by a Series of Double Proton Transfer/Double Electron Transfer/Double Proton Tautomerization (2PT/2ET/2PT)

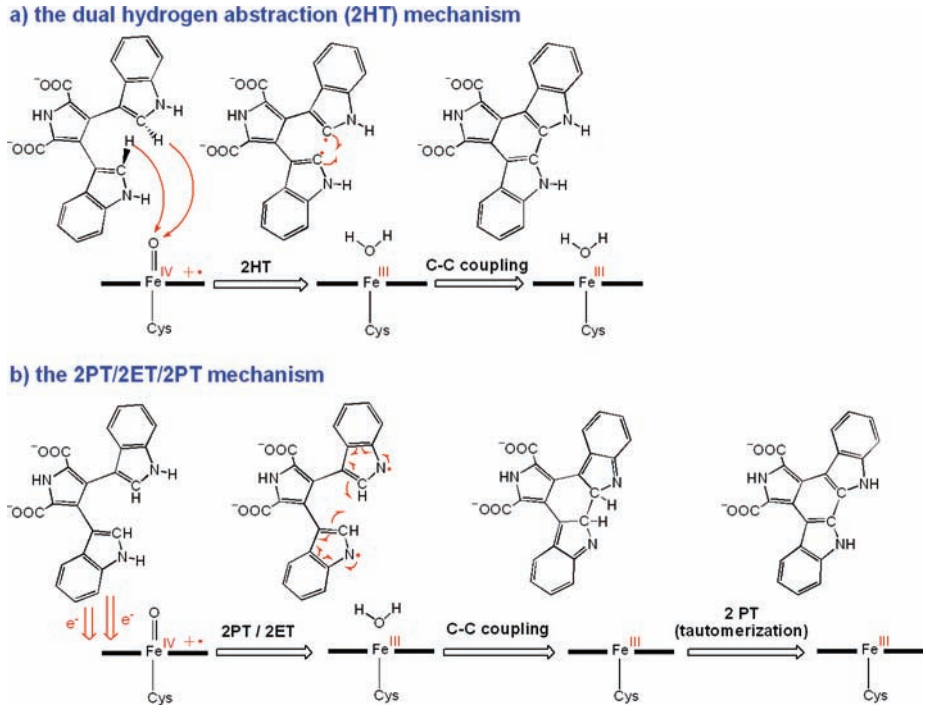


produce the final product (Scheme 3a). However, because the kinetic isotope effects were close to unity, the authors[12] concluded that the C−C coupling is not rate controlling.

On the other hand, Nagano and Onaka et al.[13] performed X-ray structure determination of the substrate-bound complex of StaP with CPA and highlighted the similarity of electrostatic potential around the indole group (proximal to the heme) of CPA to the electrostatic potential of C*c*P. This similarity led Nagano and Onaka et al. to postulate that the Cpd I(StaP)−CPA involves in fact, like C*c*P,[3,6] a one electron reduced Cpd II and a one electron oxidized CPA. On the basis of this similarity to C*c*P, these authors suggested a mechanism, which is shown in Scheme 3b, and which commences by a loss of two protons from the indole cation radical moieties (labeled as proton transfer, PT), attended by an additional electron loss and followed by intramolecular radical coupling and with the tautomerization of the two N−C−H moieties (Scheme 3b).

However, as shown by the X-ray structures of the substrate-bound complex in Figure 1, any mechanistic hypothesis faces a stringent requirement of "transport". Thus, the structure in Figure 1 reveals that CPA is clawed by an array of hydrogen bonds (H-bonds) to the enzyme,[13] such that the C−H and N−H moieties of CPA will be much too far from either Cpd I or Cpd II to promote any one of these reactions directly. Therefore, any group-abstraction process will have to be somehow mediated indirectly, and, in addition, regeneration of the aqua complex of the resting state requires the return of the "lost protons" to the oxo group; and the question is, what is the mechanism whereby all of this can be achieved?

The preliminary QM/MM calculations performed by some of us[8] supported the postulated[13] unusual properties of the StaP Cpd I, and the similarity to C*c*P. At the same time, these calculations also revealed features that formed a basis for a novel mechanism. In this mechanism, the activation of CPA is initiated by a PCET, mediated by the acid−base machinery composed

(7) (a) Ogliaro, F.; Cohen, S.; de Visser, S. P.; Shaik, S. *J. Am. Chem. Soc.* **2000**, *122*, 12892–12893. (b) Shaik, S.; Kumar, D.; de Visser, S. P.; Altun, A.; Thiel, W. *Chem. Rev.* **2005**, *105*, 2279–2328. (c) Kim, S. H.; Perera, R.; Hager, L. P.; Dawson, J. H.; Hoffman, B. M. *J. Am. Chem. Soc.* **2006**, *128*, 5598–5599. (d) Bathelt, C. M.; Zurek, J.; Mulholland, A. J.; Harvey, J. N. *J. Am. Chem. Soc.* **2005**, *127*, 12900–12908. (e) Harvey, J. N.; Bathelt, C. M.; Mulholland, A. J. *J. Comput. Chem.* **2006**, *27*, 1352–1362. (f) Stone, K. L.; Behan, R. K.; Green, M. T. *Proc. Natl. Acad. Sci. U.S.A.* **2005**, *102*, 16563–16565. (g) Schöneboom, J. C.; Neese, F.; Thiel, W. *J. Am. Chem. Soc.* **2005**, *127*, 5840–5853. (h) Rydberg, P.; Sigfridsson, E.; Ryde, U. *J. Biol. Inorg. Chem.* **2004**, *9*, 203–223. (i) Kamachi, T.; Yoshizawa, K. *J. Am. Chem. Soc.* **2003**, *125*, 4652–4661. (j) Radon, M.; Broclawik, E. *J. Chem. Theory Comput.* **2007**, *3*, 728–734. (k) Alfonso-Prieto, M.; Borovik, A.; Carpena, X.; Murshudov, G.; Melik-Adamyan, W.; Fita, I.; Rovira, C.; Loewen, P. C. *J. Am. Chem. Soc.* **2007**, *129*, 4193–205.
(8) Wang, Y.; Hirao, H.; Chen, H.; Onaka, H.; Nagano, S.; Shaik, S. *J. Am. Chem. Soc.* **2008**, *130*, 7170–7171.
(9) (a) Sanchez, C.; Mendez, C.; Salas, J. A. *Nat. Prod. Rep.* **2006**, *23*, 1007–1045. (b) Omura, S.; Sasaki, Y.; Iwai, Y.; Takeshima, H. *J. Antibiot. (Tokyo)* **1995**, *48*, 535–548.
(10) (a) Howard-Jones, A. R.; Walsh, C. T. *J. Am. Chem. Soc.* **2006**, *128*, 12289–12298. (b) Onaka, H.; Taniguchi, S.; Igarashi, Y.; Furumai, T. *J. Antibiot.* **2002**, *55*, 1063–1071. (c) Sanchez, C.; Zhu, L. L.; Brana, A. F.; Salas, A. P.; Rohr, J.; Mendez, C.; Salas, J. A. *Proc. Natl. Acad. Sci. U.S.A.* **2005**, *102*, 461–466. (d) Asamizu, S.; Kato, Y.; Igarashi, Y.; Furumai, T.; Onaka, H. *Tetrahedron Lett.* **2006**, *47*, 473–475. (e) Onaka, H.; Asamizu, S.; Igarashi, Y.; Yoshida, R.; Furumai, T. *Biosci. Biotechnol. Biochem.* **2005**, *69*, 1753–1759. (f) Salas, A. P.; Zhu, L.; Sanchez, C.; Brana, A. F.; Rohr, J.; Mendez, C.; Salas, J. A. *Mol. Microbiol.* **2005**, *58*, 17–27.
(11) (a) Onaka, H.; Taniguchi, S.; Igarashi, Y.; Furumai, T. *Biosci. Biotechnol. Biochem.* **2003**, *67*, 127–138. (b) Sanchez, C.; Butovich, I. A.; Brana, A. F.; Rohr, J.; Mendez, C.; Salas, J. A. *Chem. Biol.* **2002**, *9*, 519–531.
(12) Howard-Jones, A. R.; Walsh, C. T. *J. Am. Chem. Soc.* **2007**, *129*, 11016–11017.
(13) Makino, M.; Sugimoto, H.; Shiro, Y.; Asamizu, S.; Onaka, H.; Nagano, S. *Proc. Natl. Acad. Sci. U.S.A.* **2007**, *104*, 11591–11596.

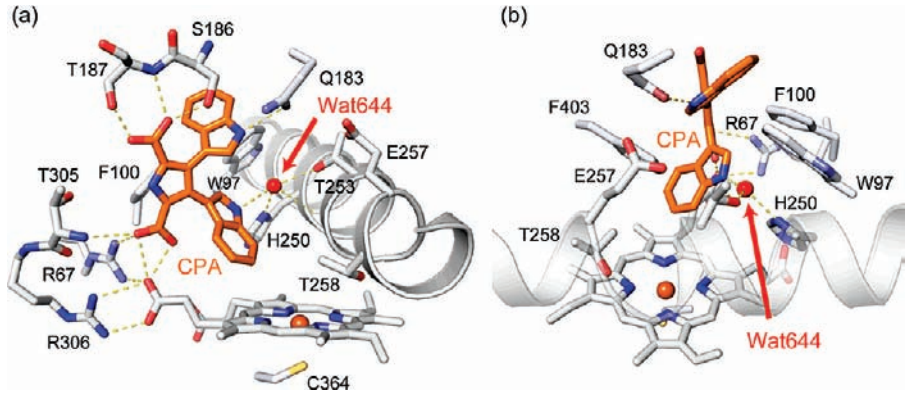


***Figure 1.*** Perspectives of the P450 StaP−CPA complex revealed by X-ray structure determination (ref 13). (a) The network of H-bonds holding CPA is indicated by the dotted lines. (b) The H-bond connection of $His_{250}$ to $Wat_{644}$ and CPA.

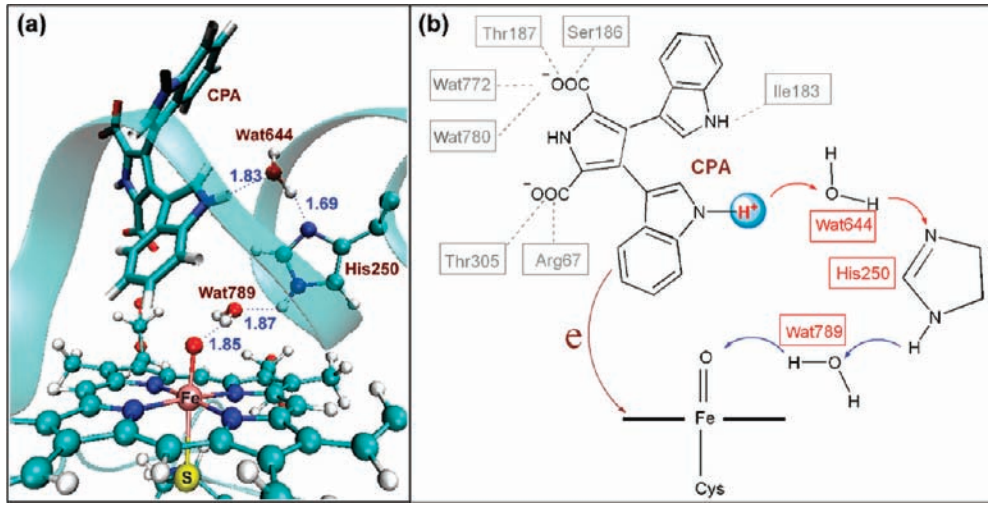


***Figure 2.*** (a) The complex of P450 StaP Cpd I with CPA. (b) A schematic initiation of the CPA activation by proton-coupled electron transfer (PCET).[8]

of the histidine residue ($His_{250}$) and two water molecules ($Wat_{644}$, $Wat_{789}$), in a manner similar to the oxidation of ferulic acid by the HRP enzyme.[4] The structure near the active site and a schematic representation of the initiation PCET step are shown in Figure 2a and b, using Cpd I as the active species. We note that the crystal water molecule, $Wat_{644}$, is present in the crystal structure of the StaP−CPA complex (Figure 1).[13] However, the second water molecule labeled as $Wat_{789}$ was not present in the same X-ray structure, because it is the water molecule that liberated only after the O−O bond activation that leads to Cpd I.[14] Notably, the analogue of $Wat_{789}$ in P450cam was shown recently to play a key role in the barrier lowering during camphor hydroxylation.[15] Indeed, as was reported in a preliminary communication,[8] $Wat_{789}$ plays a major role in the activation of CPA, and in its absence the PCET process in Figure 2b could not be completed.

There remains, however, a host of mechanistic uncertainties on the whole C−C coupling process, which involves two proton and two electron transfers: First, to continue past the initial PCET step, the proton located at the N-4′ position of the distal indole of CPA has to be transferred to the heme moiety. Yet, this N′−H bond is much too far to be directly transferred to the heme moiety. *How can this long-range proton transfer from the indole moiety to the heme actually transpire?* Would the C−C bond formation be coupled to the second electron transfer that must attend the overall transformation? Also, finally, the direct proton jumps from C-5/C-5′ to the vacant N-4/N-4′ positions (Scheme 3), encountered in the preliminary QM study[8] (Figure S16 in the Supporting Information) as huge barriers, so could these intramolecular proton jumps be also water-assisted processes as the initial PCET step (Figure 2)?

To resolve these uncertainties, we studied the entire mechanism by theoretical QM/MM methods. The major mechanistic features were tested by mutagenesis experiments and crystal structure determination of the P450 StaP−CPA and CCA complexes, which support the key elements of the mechanistic proposal. This comprehensive study is reported herein, where we demonstrate how, past the initial activation by PCET, the peroxidase-like machinery of P450 StaP and the crystal waters ($Wat_{789}$ and $Wat_{644}$) rearrange and cause C−C coupling by a bond-formation coupled electron-transfer (BFCET) mechanism and the loss of two H atoms, thus enabling the enzyme to come full circle and regenerate the resting state. Our findings underscore *the utmost importance of the crystal water as a "catalytic element" that mediates the long-range processes,*

(14) Schlichting, I.; Berendzen, J.; Chu, K.; Stock, A. M.; Maves, S. A.; Benson, D. E.; Sweet, B. M.; Ringe, D.; Petsko, G. A.; Sligar, S. G. *Science* **2000**, *287*, 1615–1622.
(15) (a) Altun, A.; Shaik, S.; Thiel, W. *J. Comput. Chem.* **2006**, *27*, 1324–1337. (b) Altun, A.; Guallar, V.; Friesner, R. A.; Shaik, S.; Thiel, W. *J. Am. Chem. Soc.* **2006**, *128*, 3924–3925.

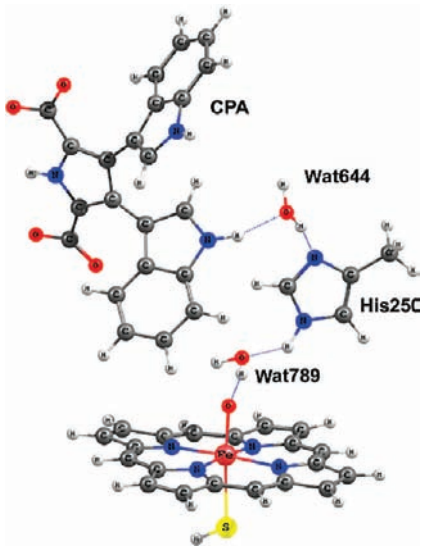


***Figure 3.*** The QM subsystem (100 atoms) used during the QM/MM calculations.

*along with the powerful electron-accepting capability of the heme that enables one to couple electron-transfer events to group transfers and bond reorganization.*

## The Computational and Experimental Methodology

**A. The Computational Part. QM/MM: Systems, Procedures, and Software.** The QM/MM procedure used here was recently reviewed.[16] The specific setup and general QM/MM methodology adopted here were described extensively in the past,[17] and in the Supporting Information of ref 8 and of the present Article. Here, we addressed only the essential features.

As shown in our preliminary study,[8] the most reasonable protonation state of the substrate is $CPA^{2-}$, where the two carboxylic groups of CPA are deprotonated. First, the geometric features fit a deprotonated CPA, and, second, using $CPA^{1-}$ leads to much higher barriers during the PCET step and is hence a dead end. As such, the QM part, shown in Figure 3, contains 100 atoms, which involve a $CPA^{2-}$ substrate and Cpd I without the peripheral substituents and with an SH axial ligand. To these we added $Wat_{644}$, part of $His_{250}$ ($Phe_{250}$ for the H250F mutant discussed later), and $Wat_{789}$. As we mentioned above, $Wat_{789}$ represents the water molecules that are liberated during the formation of Cpd I, and because it cannot be present in the structure of the resting state, it was added manually to the Cpd I structure in Figure 3.[8,15a] Because this water is generated internally during the catalytic cycle, during protonation and activation of $O_2$,[1,2] $Wat_{789}$ belongs to the natural state of the Cpd I/StaP complex, and we need not be concerned about the cost of bringing an additional water from the bulk to the active site.

This QM part is treated by density functional theory (DFT), while the rest of the protein and the additives (e.g., water molecules) are treated by MM. The QM(DFT)/MM calculations were done using ChemShell[18] interfaced to Turbomole[19] and DL_POLY,[20] which together handle the QM(DFT) and MM calculations. The UB3LYP functional[21] was used for the QM(DFT) part, and the CHARMM22 force field[22] was used for the MM part throughout the work. The active region of the protein, which is described by UB3LYP, interacts with the rest of the protein (MM part) by electrostatic and Lennard-Jones interactions; no cutoff is applied. The electronic embedding scheme was used to account for the polarization effect of the QM part induced by the protein environment. The dangling bond at the QM−MM boundary was capped by a hydrogen-link atom, and corrective terms were added by the charge-shift method.[23]

**Setup of the Model System.** To prepare a suitable initial structure for the QM/MM calculations, we started from the experimental X-ray structure of StaP in the CPA-bound state (Brookhaven Protein Database, PDB code: 2Z3U). The structure of the H250F mutant had been reconstructed by directly replacing histidine with phenylalanine by means of DeepView software.[24]

After the missing hydrogen atoms and solvent (water) were added, the entire system consisted of 24 888 (24 892 for H250F mutant model system) atoms, including 17 736 atoms in the solvent (water). The resulting structure was then relaxed by a series of energy minimizations and molecular dynamic (MD) simulations that were done using the CHARMM force field as implemented in the CHARMM program.[25] The positions of the hydrogen atoms were optimized using the CHARMM program (2400 steps of steepest descent for hydrogen atoms of the crystallographic water only, followed by 2400 steps of steepest descent for all hydrogen atoms). A water layer of 16 Å in thickness was constructed around the enzyme using the Insight II (from Accelrys, San Diego, CA) software. The inner 8 Å of the solvent layer was equilibrated (3 ps at 300 K) while keeping the remainder of the system fixed. Because the water density in the solvent layer was too low after the water molecules had

(16) Senn, H. M.; Thiel, W. *Top. Curr. Chem.* **2007**, *268*, 173–290.
(17) (a) Schöneboom, J. C.; Lin, H.; Reuter, N.; Thiel, W.; Cohen, S.; Ogliaro, F.; Shaik, S. *J. Am. Chem. Soc.* **2002**, *124*, 8142–8151. (b) Lin, H.; Schöneboom, J. C.; Cohen, S.; Shaik, S.; Thiel, W. *J. Phys. Chem. B* **2004**, *108*, 10083–10088. (c) Schöneboom, J. C.; Cohen, S.; Lin, H.; Shaik, S.; Thiel, W. *J. Am. Chem. Soc.* **2004**, *126*, 4017–4034. (d) Schöneboom, J. C.; Thiel, W. *J. Phys. Chem. B* **2004**, *108*, 7468–7478. (e) Altun, A.; Thiel, W. *J. Phys. Chem. B* **2005**, *109*, 1268–1280. (f) Cohen, S.; Kozuch, S.; Hazan, C.; Shaik, S. *J. Am. Chem. Soc.* **2006**, *128*, 11028–11029. (g) Altun, A.; Shaik, S.; Thiel, W. *J. Comput. Chem.* **2006**, *27*, 1324–1337. (h) Zheng, J. J.; Wang, D. Q.; Thiel, W.; Shaik, S. *J. Am. Chem. Soc.* **2006**, *128*, 13204–13215. (i) Altun, A.; Shaik, S.; Thiel, W. *J. Am. Chem. Soc.* **2007**, *129*, 8978–8987. (j) Fishelovitch, D.; Hazan, C.; Hirao, H.; Wolfson, H. J.; Nussinov, R.; Shaik, S. *J. Phys. Chem. B* **2007**, *111*, 13822–13832. (k) Hirao, H.; Cho, K. B.; Shaik, S. *J. Biol. Inorg. Chem.* **2008**, *13*, 521–530. (l) Wang, D. Q.; Zheng, J. J.; Shaik, S.; Thiel, W. *J. Phys. Chem. B* **2008**, *112*, 5126–5138.
(18) (a) Sherwood, P.; et al. *J. Mol. Struct. (THEOCHEM)* **2003**, *632*, 1–28. (b) ChemShell is a modular QM/MM program developed in the European QUASI project under the coordination of P. Sherwood (see http://www.cse.clrc.ac.uk/qcg/chemshell).
(19) Ahlrichs, R.; Bär, M.; Häser, M.; Horn, H.; Kölmel, C. *Chem. Phys. Lett.* **1989**, *162*, 165–169.
(20) Smith, W.; Forester, T. R. *J. Mol. Graphics* **1996**, *14*, 136–141.
(21) (a) Becke, A. D. *J. Chem. Phys.* **1992**, *96*, 2155–2160. (b) Becke, A. D. *J. Chem. Phys.* **1992**, *97*, 9173–9177. (c) Becke, A. D. *J. Chem. Phys.* **1993**, *98*, 5648–5652. (d) Lee, C.; Yang, W.; Parr, R. G. *Phys. Rev. B* **1988**, *37*, 785–789.
(22) Mackerell, A. D., Jr.; et al. *J. Phys. Chem. B* **1998**, *102*, 3586–3616.
(23) (a) Bakowies, D.; Thiel, W. *J. Phys. Chem.* **1996**, *100*, 10580–10594. (b) Sherwood, P.; de Vries, A. H.; Collins, S. J.; Greatbanks, S. P.; Burton, N. A.; Vincent, M. A.; Hillier, I. H. *Faraday Discuss.* **1997**, *106*, 79–92. (c) de Vries, A. H.; Sherwood, P.; Collins, S. J.; Rigby, A. M.; Rigutto, M.; Kramer, G. J. *J. Phys. Chem. B* **1999**, *103*, 6133–6141.
(24) Guex, N.; Peitsch, M.; Schwede, T.; Diemand, A. *DeepView. Swiss PDB Viewer*; Glaxo Smith Klein.
(25) Brooks, B. R.; Burccoleri, R. E.; Olafson, B. D.; States, D. J.; Swaminathan, S.; Karplus, M. *J. Comput. Chem.* **1983**, *4*, 187–217.

adapted to the enzyme surface, more water molecules were added to the solvent layer, and this procedure was repeated two times.

The initial topology file of the substrate (double-deprotonated CPA, $CPA^{2-}$ in brief) was generated by Insight II 2000, and the force field parameters were taken first from those of known amino acids Asp, His, and Trp residues. The charges of carbons in the pyrrole ring were determined so that the total charge of the tail of CPA, the carboxyl, and pyrrole group ($^-$OOC−pyrrole−COO$^-$) is −2. The resulting topology and related parameter set for $CPA^{2-}$ are presented in Figure S3 in the Supporting Information of ref 8. PROPKA[26] was used in combination with additional visual inspection to assign the protonation states of titratable residues.

The protonation states were defined then as follows: (i) $Glu_{257}$ and $Glu_{373}$ were protonated at the carboxylate side chain; and (ii) $His_{362}$ and $His_{404}$/($His_{250}$ and $His_{256}$) were protonated at the $\varepsilon$/($\delta$) nitrogen and the others at both nitrogens.

**The QM/MM Calculations.** The QM/MM optimizations included the residues within 2.4 Å from $CPA^{2-}$ and the Cpd I parts of the QM system and other key residues mentioned in ref 13: $Arg_{67}$, $Trp_{97}$, $Val_{l99}$, $Phe_{100}$, $His_{106}$, $Arg_{110}$, $Ile_{161}$, $Gln_{183}$, $Ser_{186}$, $Thr_{187}$, $Leu_{198}$, $His_{250}$, $Ala_{254}$, $Thr_{258}$, $Thr_{259}$, $Met_{295}$, $Pro_{300}$, $Val_{301}$, $Val_{304}$, $Thr_{305}$, $Arg_{306}$, $Gly_{356}$, $Phe_{357}$, $His_{362}$, $Tyr_{363}$, $Cys_{364}$, $Leu_{365}$, $Gly_{366}$, $Ala_{367}$, $Leu_{369}$, $Ala_{370}$, $Phe_{403}$, $HEM_{500}$, $CRR_{501}$, $Wat_{618}$, $Wat_{627}$, $Wat_{644}$, $Wat_{702}$, $Wat_{703}$, $Wat_{772}$, $Wat_{776}$, $Wat_{780}$, and $Wat_{789}$ (the newly added molecule). The total number of atoms in the geometry optimization was 663 atoms for $CPA^{2-}$ and 664 atoms in the case of the monodeprotonated substrate, $CPA^{1-}$ in total. The total charge of the system was −2.

Geometry optimizations were performed with the HDLC optimizer.[27] All minima points were fully optimized without symmetry constraint. Full TS optimization that employed a rational function optimizer with the Powell update (P-RFO) for an explicit Hessian did not converge because of the large and flexible QM regions, and thus all transition state points were taken to be the highest point on the potential energy profile along the reaction coordinate, which was scanned with an increment of 0.02 Å for the C−C coupling step and 0.005 Å for the PCET step, near the transition state points. A two-dimensional (2D) scan of the second step in the PCET mechanism verified that the procedure is reliable.[8] We note that the barrier at the level of geometry optimization (basis set B1; see below) is 12.0 kcal/mol (see Figure S27 in the Supporting Information of ref 8), and when zero-point energy (ZPE) correction is considered, the barrier will be lowered by ca. 4 kcal/mol. This is still on the high side of proton-transfer barriers, and it may reflect the fact that the process is leading to a doubly protonated His250, which is an endothermic process. In addition, because the 1D/2D scan gave a similar energy barrier, and because a 2D scan was too time-consuming, we only performed the 1D scan in the following steps of the mechanism.

The scanned reaction coordinates in each step are listed as the following: (i) **s1**(PCET), $H_{CPA}-O_{wat644}/H_{His250}-O_{wat789}$ (Figure S2); (ii) **s3**(PT1), $H_{CPA}-O_{wat644}$ (Figure 6b−d); (iii) **s4**(BFCET), $C5_{CPA}-C5'_{CPA}$; (iv) **s6**(PT2), $H_{CPA}-O_{wat644}$ (Figure S8b−d); (v) **s8**(PT3), $H_{C5}-O_{wat789}$ (Figure S10b−d); (vi) **s10**(PT4), $H_{C5'}-O_{wat644}$ (Figure S10f−h).

The basis set of the QM part, during geometry optimization, is the commonly used one, having a small-core ECP together with the double-$\zeta$ quality LACVP basis set on the iron atom, and 6-31G basis set for all other atoms (H, C, N, S, O), hence B1 in brief. The energy was corrected by a single point energy calculation on the B1 geometry, using a TZVP basis set,[28] B2 in brief. The total number of basis functions in B2 is 1449.

**Water Rearrangement.** As we shall see later, the mechanism involves water-chain relocation steps (see Scheme 4), which occur over long distance (∼5.0 Å) and involve coupled movement of 2−3 water molecules. These processes require accurate MD simulations and/or full dimensional potential energy searches, which are too time-consuming (impossible) for this large and complex model system. As such, probing the water movement is limited to the study of the initial and final states in each step. For an assessment of such barriers in a typical water-relocation event, we performed a scan for one of the water-relocation steps, **s2** (Figure S4). It is noteworthy that the different water-relocation steps have different hydrogen-bonding situations, and hence their barriers, if they could be computed, may also be different.

**B. The Experimental Part. X-ray Crystallography.** The enzyme was expressed and purified according to the previously reported procedures.[13] The purified protein sample (60 mg/mL) was mixed with an equal volume of 4 mM CCA and then incubated at 4 °C for 1 h. The CCA (Scheme 2b)-bound StaP was crystallized using sitting drop, vapor diffusion method. Single crystals were obtained by using 8% PEG4000, 50 mM Bis-Tris pH 6.8, 50 mM $MgCl_2$, 40 mM $MnCl_2$ as a reservoir solution at 20 °C. The crystals were cryo-protected by the reservoir solution containing 20% ethylene glycol and used for the diffraction experiment. The diffraction data were collected using the ADSC Quantum 210 CCD detector in BL44B2 at SPring-8. The HKL2000 program[29] was used for integration of the diffraction intensity and scaling.

5% of the observed reflections were selected as a test set for the cross-validation[30a] to match the test set for CPA-bound StaP and kept during all refinement steps. The program CNS[30b] was used for the refinement. The structure of CCA-bound StaP was first obtained by rigid body refinement using the CPA-bound StaP as an initial model.[30c] In the first stage of the model refinement, a simulated annealing protocol was employed. The model was further refined with a position and individual *B* factor refinement with a resolution range of 20−2.5 Å. After a few rounds of refinement, the $F_o - F_c$ map shows positive density at the substrate binding site. A CCA molecule was reasonably fitted into the positive electron density. Parameter and topology files of the CCA for the program were generated by PRODRG server.[30d] Analysis of this enzyme geometry was performed with the programs Procheck[30e] and Whatcheck.[30f] Almost all main-

(26) Li, H.; Robertson, A. D.; Jensen, J. H. *Proteins* **2005**, *61*, 704–721.
(27) Billeter, S. R.; Turner, A. J.; Thiel, W. *Phys. Chem. Chem. Phys.* **2000**, *2*, 2177–2186.
(28) (a) Schäfer, A.; Huber, C.; Ahlrichs, R. *J. Chem. Phys.* **1994**, *100*, 5829–5835. (b) Schäfer, A.; Horn, H.; Ahlrichs, R. *J. Chem. Phys.* **1992**, *97*, 2571–2577.
(29) Otwinowski, Z.; Minor, W. *Methods Enzymol.* **1997**, *276*, 307–326.
(30) (a) Brunger, A. T. *Nature (London)* **1992**, *355*, 472–475. (b) Brunger, A. T.; Adams, P. D.; Clore, G. M.; DeLano, W. L.; Gros, P.; Grosse-Kunstleve, R. W.; Jiang, J. S.; Kuszewski, J.; Nilges, M.; Pannu, N. S.; Read, R. J.; Rice, L. M.; Simonson, T.; Warren, G. L. *Acta Crystallogr., Sect. D* **1998**, *54*, 905–921. (c) Brunger, A. T.; Adams, P. D.; Clore, G. M.; DeLano, W. L.; Gros, P.; Grosse-Kunstleve, R. W.; Jiang, J. S.; Kuszewski, J.; Nilges, M.; Pannu, N. S.; Read, R. J.; Rice, L. M.; Simonson, T.; Warren, G. L. *Acta Crystallogr., Sect. D* **1998**, *54*, 905–921. (d) Schuttelkopf, A. W.; van Aalten, D. M. *Acta Crystallogr., Sect. D* **2004**, *60*, 1355–1363. (e) Laskowski, R. A.; MacArthur, M. W.; Moss, D. S.; Thornton, J. M. *J. Appl. Crystallogr.* **1993**, *26*, 283–291. (f) Hooft, R. W. W.; Vriend, G.; Sander, C.; Abola, E. E. *Nature (London)* **1996**, *381*, 272–272.

***Scheme 4.*** Comprehensive Mechanism of C−C Coupling of CPA by StaP

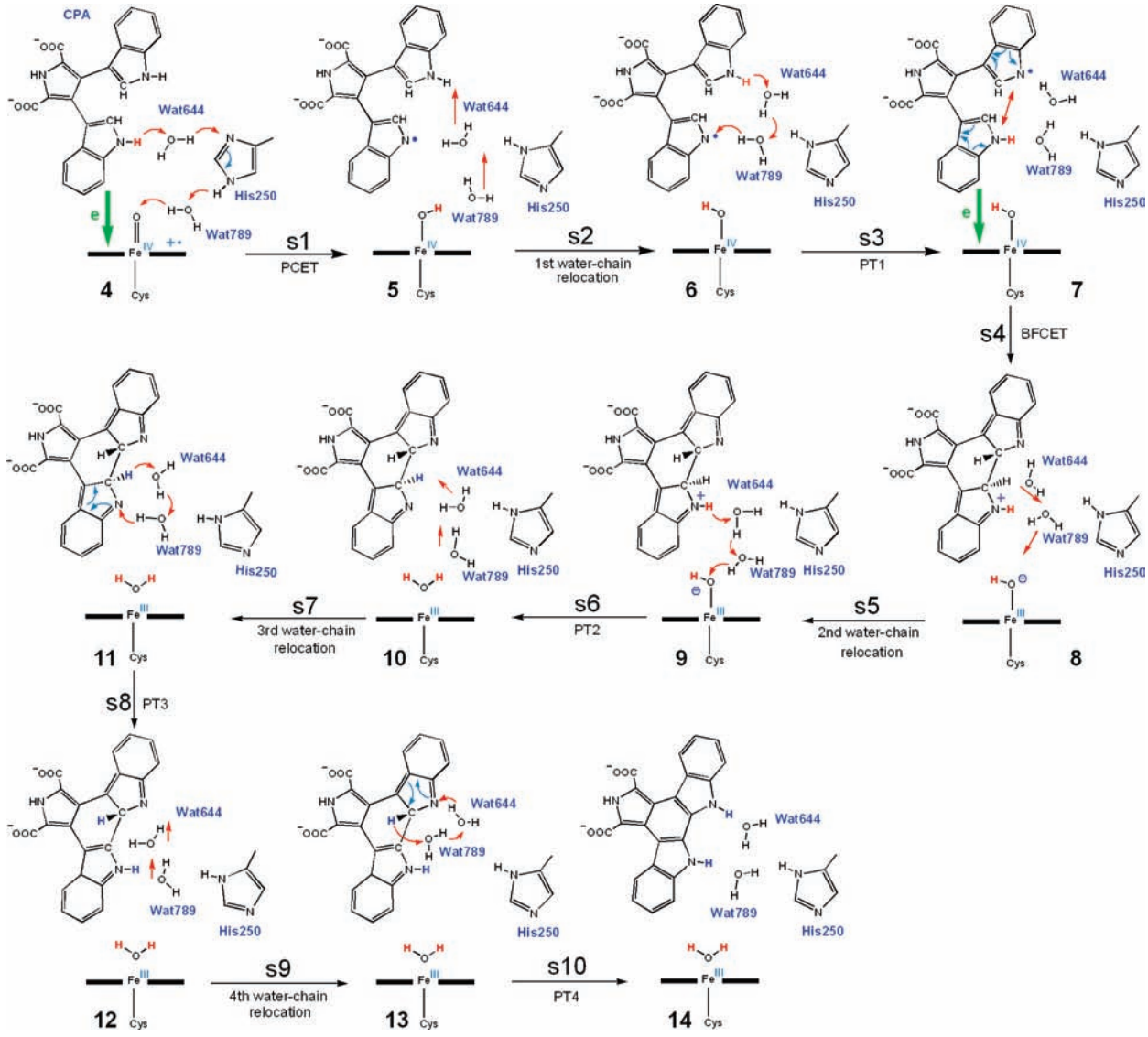


chain dihedral angles were in the allowed and additional allowed region of Ramachandran plot. The data collection and refinement statistics are summarized in Supporting Information Table S7.

**Site-Directed Mutations: (1) Expression and Purification of StaP and RebP Used for the Enzyme Assay.** The wild-type (WT) and mutant P450 StaPs used for the enzymatic activity assay were expressed as C-terminal hexahistidine-tagged fusion proteins in *Escherichia coli* BL21(DE3) under the control of T7 RNA polymerase promoter. The expression vector for StaP was pETstaP (ref 13), and the vectors for the StaP mutants were pETstaP-H250A and pETstaP-H250F. Detailed conditions on the expression vector construction and purification of StaP and RebP are described in the Supporting Information.

**Site-Directed Mutations: (2) Enzymatic Reactions.** The activities of the WT P450 StaP and its mutant enzymes were determined by examining the conversion of CPA to K252c using analytical HPLC. The reaction solution contained an enzyme (2 $\mu$M of WT StaP, H250A StaP, H250F StaP, or RebP), 260 $\mu$M CPA or CCA as the substrate, 10 $\mu$M ferredoxin (Sigma), 0.5 $\mu$M ferredoxin reductase (Sigma), and 10 mM NADH in 75 mM HEPES buffer at pH 8.0 with 1 mg/mL BSA. After incubation at 30 °C, the enzymes were inactivated by the addition of 3 volumes of methanol. The reaction mixtures were analyzed using HPLC at 268 nm, which is the maximum absorption wavelength of CPA and CCA. HPLC analysis was performed using an HP 1100 system (Hewlett-Packard) and a Cosmosil column (i.d., 4.6 mm; length, 250 mm; Nacalai Tesque). The temperature was set to 30 °C, and the flow rate was 1 mL/min. The solvent consisted of acetonitrile and 0.1% TFA in $H_2O$. Elution was performed for 30 min using a 20−90% linear gradient of acetonitrile. The amounts of CPA, CCA, and K252c were calculated from the area under the elution profile monitored at their maximum absorbance.

## Results

**A. The Nature of Cpd I−CPA Complex.** Figure 4 summarizes briefly our previous findings[8] about the nature of Cpd I in P450 StaP, in three different environments. In all of the cases, the Cpd I−CPA complex has two low lying states that are virtually degenerate, the doublet state being lower than the quartet state at the B2//B1 level by ca. 0.1 kcal/mol.[5b,17a] Furthermore, in all of the environments, two of the unpaired electrons reside in the $\pi^*$(FeO) orbitals (see Scheme 1), while the third electron occupies an orbital of a mixed $a_{2u(Por)}/\phi_{CPA}$

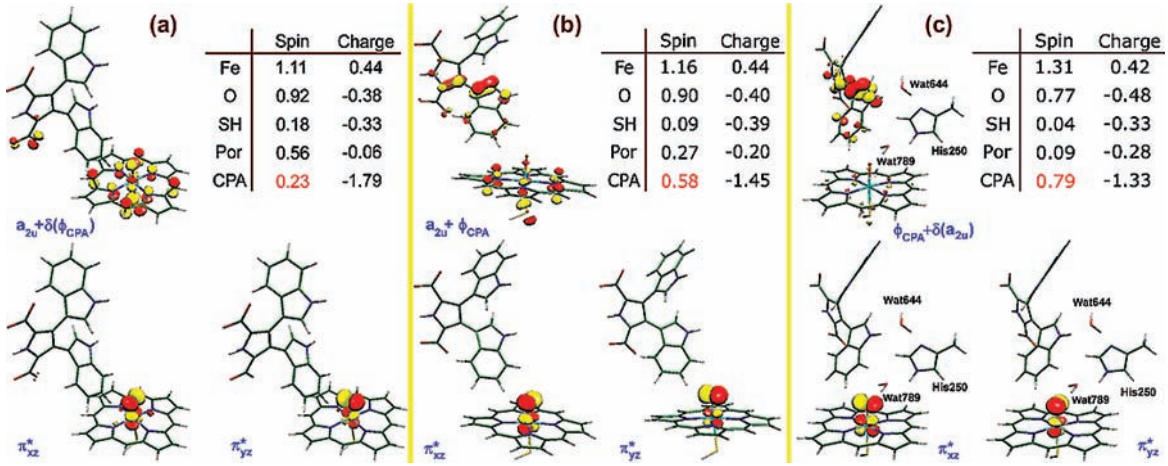


***Figure 4.*** The singly occupied orbitals and spin density distribution of the Cpd I−$CPA^{2-}$ complex at the UB3LYP(B2//B1):MM level with: (a) a distally protonated $His_{250}$, (b) a proximally protonated $His_{250}$, and (c) a proximally protonated $His_{250}$ and $Wat_{789}$.

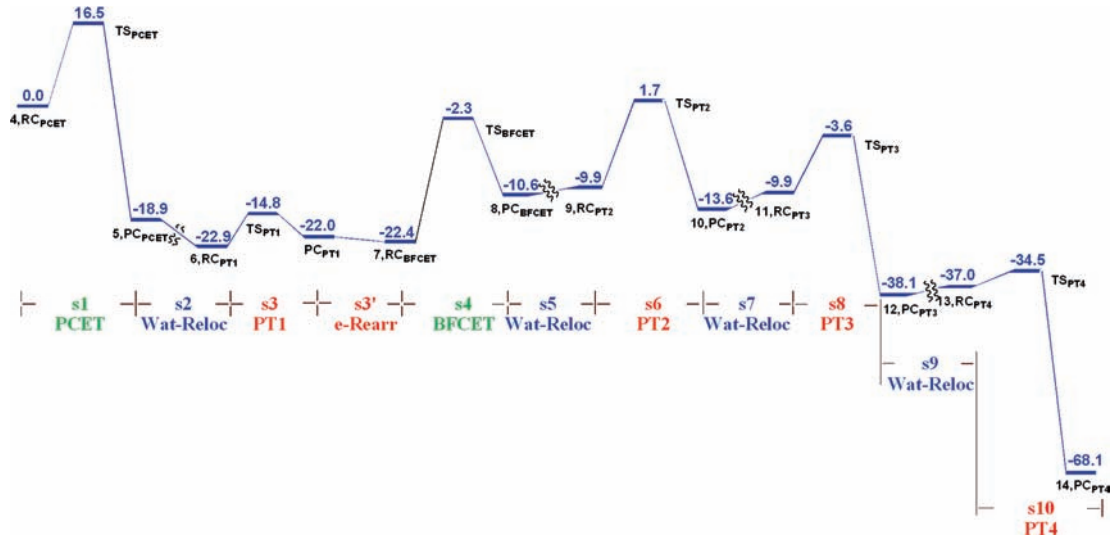


***Figure 5.*** The UB3LYP/B2//B1:MM calculated doublet-state energy profile (in kcal/mol) for the whole process of C−C coupling of CPA by P450 StaP. Studies of the water-relocation pathways were limited usually to the initial state of a given step (see methods section).

nature to a degree dependent on the environment and conformation. Thus, when the $His_{250}$ residue was protonated away from the iron-oxo moiety, in Figure 4a, the spin density on the CPA moiety was minimal, 0.26, and the $a_{2u}$ character of the heme unit dominated the singly occupied orbital. However, when $His_{250}$ was protonated at the side pointing toward the iron-oxo moiety, in Figure 4b, the spin density was now slightly more on CPA. This became dominantly so, when $Wat_{789}$ was added to assume its position after the O−O heterolytic cleavage process;[15a] now, in Figure 4c, the spin density was mostly localized on CPA, and the singly occupied orbital became almost pure indolic-CPA type. We further verified that the deleting of the partial charges of the H atoms (in residues $Ser_{186}$, $Thr_{187}$, $Arg_{67}$, and $Thr_{305}$ and in the crystal water molecules $wat_{772}$ and $wat_{780}$) that are H-bonded to the distal carboxylate of CPA moved most of the spin density >0.9 to CPA.

Clearly, therefore, the QM/MM results demonstrated that the H-bonding network of the protein controls and modulates the extent of electron transfer (ET) from $CPA^{2-}$ to Cpd I and supported the hypothesis that the StaP Cpd I is analogous to the one found in C*c*P.[13] However, the calculations also highlighted the dynamic chameleon nature of Cpd I.[5a] Thus, strong H-bonds with the distal carboxylate dampened the extent of ET, while creating an H-bond path between CPA and the iron-oxo via the $Wat_{644}$−$His_{250}$−$Wat_{789}$ triad (Figure 4c) that enhanced the ET from CPA to generate a Cpd II species analogous to C*c*P. Hence, the electronic nature of Cpd I−$CPA^{2-}$ will be dynamic, and its hybrid nature will depend on the fluctuations of the protein. Nevertheless, in all cases, the generation of the Cpd II−$CPA^{1-}$ situation, by full ET, is going to be rather facile. This ET from $CPA^{2-}$ to Cpd I may activate CPA and will initiate the eventual C−C bond formation, en route to STA production (Scheme 2). This mechanism is described in the next subsection.

**B. A Bird's Eye View of the Whole Reaction Process. Mechanistic Scheme.** Starting from the Cpd I−CPA structure in Figure 4c, we explored the mechanism that leads to the C−C coupling process. The entire mechanism is composed of 10 distinct steps, which are labeled as **s1**−**s10** in Scheme 4. The mechanistic scheme can be subdivided into two major parts. The first part involves the intermolecular proton/electron-transfer events from the substrate CPA to the heme moiety of StaP (steps **s1**−**s6**), and the second part involves only water-assisted intramolecular proton rearrangement events within the substrate (steps **s7**−**s10**). Figure 5 provides the B2//B1 energy profile corresponding to this mechanistic scheme.

As discussed above, the Cpd I−CPA complex, **4** (Scheme 4), involves an incomplete electron transfer from the deprotonated CPA to the porphyrin of the heme moiety, and the ground state is a hybrid of the indole-cation radical-CPA/Cpd II and CPA/Cpd I forms. The complete electron transfer is accomplished by a PCET mechanism mediated via the $Wat_{644}$−$His_{250}$−$Wat_{789}$ triad (**s1**, Scheme 4), and it leads to the formation of **5** with Fe(IV)OH heme moiety and a radical on the N4 position of the proximal indole moiety of CPA. Our 2D scan (see Figure S2 in the Supporting Information) shows that this process is close to being effectively concerted,[8] although we could not rule out a stepwise mechanism with a tiny barrier for the final proton transfer to the iron-oxo.

The distance between the proton located at N-4′ position in the distal indole and the FeOH group of the heme moiety **5** is much too far for direct transfer of the N−4′ proton. To enable this transfer, a water-chain relocation event must occur first as shown in **s2** leading to structure **6**, which is prepared for proton transfer via the chain distal indole→proximal indole described in **s3** and leading to structure **7**. Interestingly, **7** appears in two closely lying electromers, one PorFe(IV)OH directly formed in the PT1 process, and the other is $Por^{+\bullet}$Fe(III)OH (see discussion later), which initiates the C−C coupling step. Thus, the newly protonated indole in **7** is susceptible to radical attack by the distal indolyl radical, thereby leading to the C−C bond formation step (**s4**) and generation of structure **8**, which is typified by a protonated N−H. Importantly, the C−C bond formation is attended by a second electron transfer from the substrate to the heme, and therefore **s4** involves a novel bond-formation coupled electron-transfer (BFCET) process, as first observed in the photochemistry by Goodman et al.[31a] This BFCET process is distinct in the sense that the C−C bond formation occurs in an intramolecular fashion, that is, within the substrate, while the coupled long-range electron transfer occurs intermolecularly, that is, from the substrate to the heme moiety of StaP. There exist analogous BFCET processes, for example, in the traditional oxygen rebound process in alkane hydroxylation by P450[7a] and MMO.[31b] In these processes, however, the C−O bond formation and the coupled electron transfer are both intermolecular. Thus, *the present BFCET is the first description of an intramolecular bond-formation-coupled intermolecular electron-transfer process in a biosystem.*

At this stage of structure **8**, the heme has already been reduced by two electrons, and it received one proton that was relayed from the substrate CPA by the $Wat_{644}$−$His_{250}$−$Wat_{789}$ triad. To transfer the second and last proton to the heme-oxo moiety, a second water-chain relocation must occur to generate a proton relay pathway between proximal indole N−H in **8** and the heme moiety; this is described by step **s5** leading to structure **9** in Scheme 4. Structure **9** possesses the requisite water chain to mediate the second proton transfer in step **s6** and generate structure **10**. At this point, the cycle has come full circle and has regenerated the resting state of the heme, which is a ferric−aqua complex. However, the substrate in **10** is still not yet in its final desired form (structure **14**). This is achieved in the second part of the mechanism (**s7**−**s10**) where the water molecules shuttle back and forth to catalyze the rearrangement of the substrate from **11** to **14**.

To effect this transformation, the hydrogens on the $C_\alpha$−H bonds of **10** have to shift to the indolic nitrogens. However, from previous experience, direct rearrangement from $C_\alpha$ to the corresponding vacant nitrogen position has a very high barrier due to a highly strained transition state. This strain can be relieved if the water molecules can mediate the rearrangement.[32] This mediation requires two water-chain relocation steps, **s7** and **s9**, to occur and thereby generate a proton relay pathway for these intramolecular proton transfers, which follow in steps **s8** and **s10**. Subsequently, the substrate regains its aromatic structure in **14** and is ready for the subsequent decarboxylation step, which may occur in a nonenzymatic manner[10b] and is not studied here.

**Energy Profiles.** The energy profile corresponding to the above mechanistic scheme is shown in Figure 5, and it involves only the doublet-spin state mechanism, because the doublet state becomes definitely the lower state along the path. Thus, throughout the mechanism the doublet is only slightly lower than the quartet, but at the junction of the C−C bond closure (**s4**), which is rate determining, the two states bifurcate, the doublet being significantly lower for reasons to be explained later. As we have reported in the preliminary communication,[8] the initial PCET step (**s1**) is an effectively concerted process having a B2//B1 barrier of 16.5 kcal/mol and is 18.9 kcal/mol exothermic (see Figure S2 in the Supporting Information). After the first water-chain relocation (**s2**), the ensuing proton relay pathway is so efficient that the proton transfer from distal indole to the proximal one (**s3**) has a barrier of only 8.1 kcal/mol (**s3**) and generates the $\mathbf{PC}_{PT1}$ intermediate. $\mathbf{PC}_{PT1}$ is an electromer of Cpd II with a PorFe(IV)OH moiety, A very closely lying electromer is the one labeled **7**. $\mathbf{RC}_{BFCET}$ wherein the same moiety has the $Por^{+\bullet}$Fe(III)OH electronic structure, as found previously in HRP.[4] The electronic rearrangement (**s3′**) from $\mathbf{PC}_{PT1}$ to $\mathbf{RC}_{BFCET}$ involves a single electron shift from the porphyrin to the iron center. The energies of these two electromers are very close, and the barrier for the transformation is most likely very tiny as may be judged from the vertical energy gap of 5.7 kcal/mol between the two species (a single point energy of $^2\mathbf{RC}_{BFCET}$ at the geometry of $^2\mathbf{PC}_{PT1}$), which would lead to a barrier at most of 1.5 kcal/mol, using a Marcusian relationship for electron transfer.

$\mathbf{RC}_{BFCET}$(**7**) initiates the C−C bond formation step (**s4**), which is coupled to the second electron transfer, hence BFCET. Note that the $Wat_{644}$−$Wat_{789}$ diad is crucial in this step too, which occurs with a barrier of 20.1 kcal/mol, as compared to 23.4 kcal/mol if the C−C coupling barrier had occurred without the presence of the water diad (see Figure S3 in the Supporting Information). As such, *the water diad acts as a catalyst for the C−C coupling.*

Past the second water-chain relocation (**s5**), the following PT2 step (**s6**) occurs with a barrier of 11.6 kcal/mol and is exothermic. At this junction, the heme-oxo moiety is already reduced to the resting state, and the active species of the enzyme came full cycle to regenerate the resting state; cytochrome P450 StaP has thus accomplished its function. In the following intramolecular proton rearrangement steps (**s8**−**s10**), the water diad serves as a catalyst and carries out the entire transformation

(31) For BFCET in photochemical reactions, see:(a) Karki, S. B.; Dinnocenzo, J. P.; Farid, S.; Goodman, J. L.; Gould, I. R.; Zona, T. A. *J. Am. Chem. Soc.* **1997**, *119*, 431–432. (b) For BFCET during rebound in methane hydroxylation by MMO, see references for example: Siegbahn, P. E. M.; Blomberg, M. R. A. *Chem. Rev.* **2000**, *100*, 421–437. Yoshizawa, K.; Shiota, Y. *J. Am. Chem. Soc.* **2006**, *128*, 9873–9881. Torrent, M.; Vreven, T.; Musaev, D. G.; Morokuma, K.; Farkas, O.; Schlegel, H. B. *J. Am. Chem. Soc.* **2002**, *124*, 192–193. Baik, M. H.; Newcomb, M.; Friesner, R. A.; Lippard, S. J. *Chem. Rev.* **2003**, *103*, 2385–2419.

(32) Wang, Y.; Kumar, D.; Yang, C. L.; Han, K. L.; Shaik, S. *J. Phys. Chem. B* **2007**, *111*, 7700–7710.

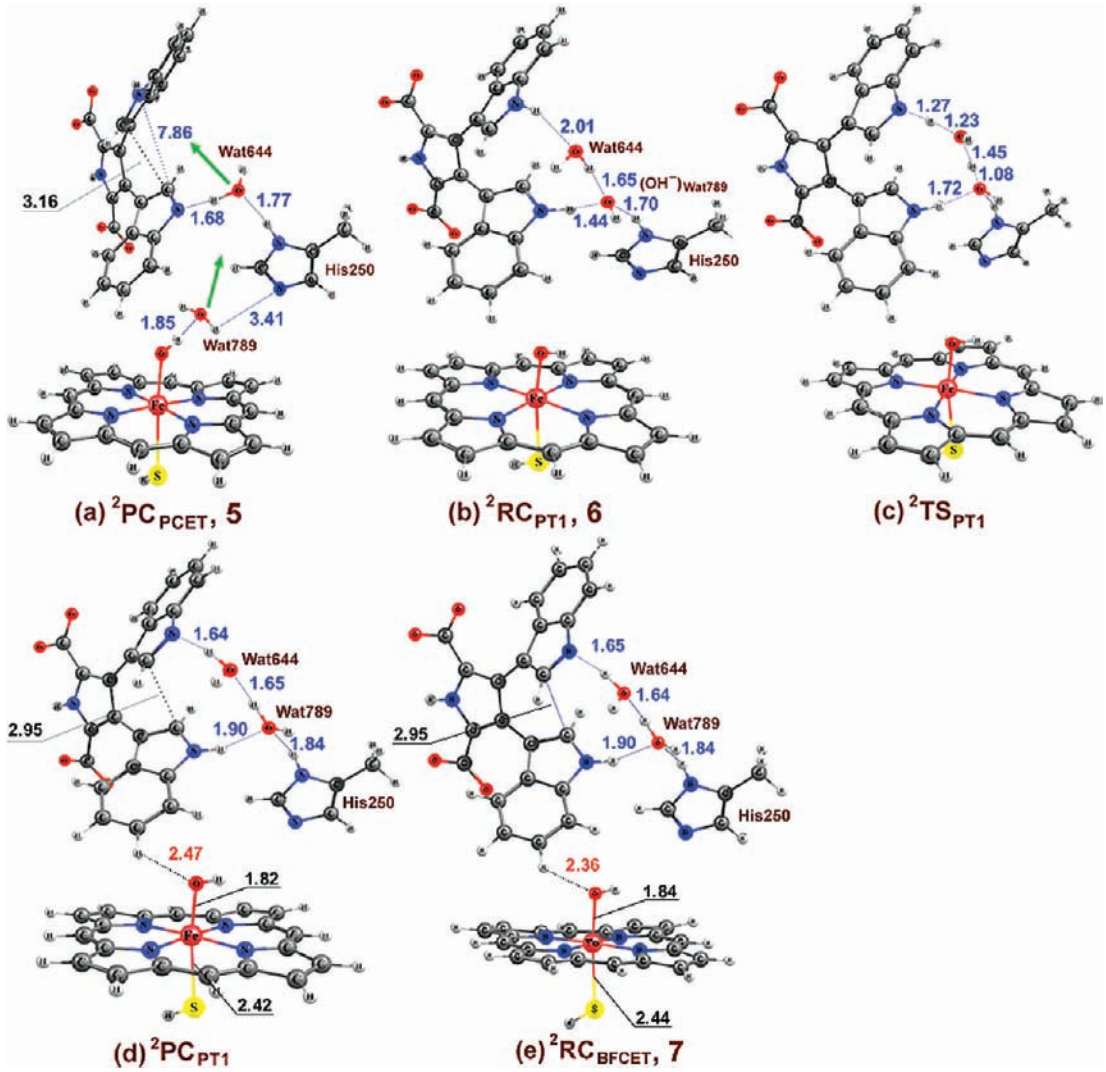


***Figure 6.*** UB3LYP(B1)/MM-optimized key geometric parameters of the intermediates and transition states involved in the first water relocation and the subsequent PT1 steps (**s2** and **s3**). Distances are in angstroms.

with a maximal barrier of 6.3 kcal/mol. The entire process is highly exothermic, and because the protein environment is expected to absorb the excess energy quickly, the C−C bond formation in the BFCET step (**s4**) has the largest barrier in this mechanism. Because we cannot obtain accurate barriers for the water-relocation steps and because the barrier of the water-chain relocation appears to be of the same order as the barriers of the other steps (see below), we cannot rule out that these steps will impact the rate of the catalytic cycle described in Figure 5 and Scheme 4. However, we recall that without the PCET initiation (**s1**), all of the barriers are considerably higher, so we may single out the PCET step as a key to the ensuing mechanism.

**C. Transition State Structures and Electronic Features of Key Species.** There are three kinds of processes shown in Figure 5. One involves the electron-coupled processes shown in green (steps **s1** and **s4**); the second consists of water-relocation and is shown in blue (steps **s2**, **s5**, **s7**, and **s9**); and the last is the water-assisted proton-transfer processes shown in red (steps **s3**, **s6**, **s8**, and **s10**). To keep a concise text that involves only mechanistic essentials, we restrict the description to one example for each process type: **s2** for water-relocation, **s3** for the subsequent water-assisted proton-transfer events, and **s4** for electron-coupled bond reorganization event. All of the data in full are relegated to the Supporting Information.

**Water-Relocation and Follow-Up PT Steps (Steps s2−s3′).** After the initial PCET step (**s1**), the proton from the distal indolic N−H has to be transferred to the heme-oxo via an initial station where the proton moved to the proximal N-indole, which is vacant in $^2$**PC**$_{PCET}$ in Figure 6a. However, the distance between the two indole moieties is far too long (7.86 Å, Figure 6a) to allow for this proton relay to occur. Also, here the water molecules come to the rescue. Thus, past the PCET step (**s1** in Scheme 4), the strong H-bond between $His_{250}$ and $Wat_{789}$ is broken (note the distance between $Wat_{789}$ and $His_{250}$ is long, ca. 3.41 Å, in Figure 6a). Consequently, now $Wat_{789}$ is able to move relatively easily and reach the proximal indole position, while pushing $Wat_{644}$ to the vicinity of the distal indole, as shown in the green arrows in $^2$**PC**$_{PCET}$ in Figure 6a. This water movement fills the space and generates **6**, $^2$**RC**$_{PT1}$ (Figure 6b), which is ready now for proton transfer from the distal N−H to the proximal N-indole en route to the ultimate transfer to the oxo-heme moiety. This occurs, however, in a stepwise manner; $Wat_{789}$ is clawed by strong H-bonding interactions with $His_{250}$ and $Wat_{644}$ as H-donors, and with the deprotonated N-4 position

***Scheme 5.*** Orbital Occupancy Changes and Relative Energies at the UB3LYP(B1)/MM Level (in kcal/mol) for $^2$**PC**$_{PT1}$ → $^2$**RC**$_{BFCET}$

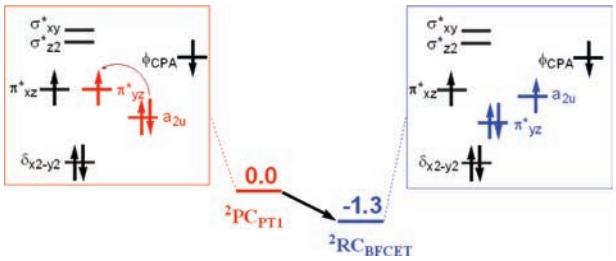


of the proximal indole. Hence, Wat$_{789}$ transfers a proton to the vacant N-4 position in the proximal indole and generates a hydroxide anion that is stabilized by three H-bonds ($^2$**RC**$_{PT1}$ in Figure 6b). Subsequently, the proton from the distal N−H moves via Wat$_{644}$ and His$_{250}$, reprotonates the hydroxide (via Figure 6c and d), and restores Wat$_{789}$ such that the net effect is a proton transfer from the distal N−H to the proximal N position, thus generating a distal N-centered radical in $^2$**PC**$_{PT1}$.

To get an approximate barrier for the water-relocation step, we carried out a one-dimensional (1D) scan on the first water-chain relocation with a low convergence criterion and coarse stepsize (0.2 Å) and obtained a barrier of 19.1 kcal/mol. Of course, a 2D scan with ultrafine step-size would have led to a barrier much lower than this, but this is computationally too demanding (although not necessarily more rigorous). Just the same, comparing the barrier of other steps shown in Figure 5, we can say that the barrier of the water-chain relocation is of the same order as the barriers of the other steps.

After the product complex $^2$**PC**$_{PT1}$ (Figure 6d), generated by the PT1 step, the water diad maintains a strong H-bonding interaction between two indole moieties and "pulls" them closer together, from 3.16 (Figure 6a) to 2.95 Å (Figure 6d). Another change that occurs is in electronic structure, as shown in Scheme 5 and Figure 6e; $^2$**PC**$_{PT1}$ possesses a closed-shell-porphyrin-Fe(IV) electronic configuration $\pi^{*1}\pi^{*1}\phi_{CPA}{}^1$. This electromer of Cpd II undergoes an electron rearrangement (**s3′**) to the more stable state $^2$**RC**$_{BFCET}$, an open-shell-porphyrin-Fe(III) electronic configuration, $\pi^{*1}a_{2u}{}^1\phi_{CPA}{}^1$, which initiates the subsequent BFCET step (recall **s4** in Scheme 4). This process that is described below in more detail is facilitated by two factors: the "pulling" together of the two indolic N moieties by the water diad, and the change of the electronic structure to $^2$**RC**$_{BFCET}$.

**The BFCET Process (Step s4).** As already stated, the BFCET step is facilitated by the "pulling" together of the two indolic N moieties (see Figure 6e) by the water diad, and by coupling the C−C bond formation to electron transfer from the CPA to the porphyrin cation radical. Without the water diad, the barrier is appreciably higher, while the coupled electron-transfer event to the heme causes spin state selectivity. The latter aspect is discussed below.

The electron transfer to the heme is apparent by inspecting the spin density changes during the process starting from **RC**$_{BFCET}$, which appears in two very closely lying spin states, doublet and quartet. On the quartet state, the spin density on the FeOH moiety (Figure S6) rises from 2.24 ($^4$**RC**$_{BFCET}$) to 2.95 ($^4$**PC**$_{BFCET}$), while on the doublet state, the spin density on the combined porphyrin/thiolate moiety changes from 0.95 ($^2$**RC**$_{BFCET}$) to almost zero ($^2$**PC**$_{BFCET}$). These changes correspond to the following electron shifts shown in Scheme 6.

Thus, in the quartet state, the electron initially in the CPA orbital $\phi_{CPA}$, which is localized on the distal indolic N (**7**, in Scheme 4), shifts to the $\sigma^*_{z^2}$ orbital of the Fe(IV)OH moiety of $^4$**RC**$_{BFCET}$, and thereby causes a rise of the spin density from two to three spins. By contrast, in the doublet state, the electron is shifted to the $a_{2u}$ orbital of the porphyrin and thereby diminishes the spin on this moiety. These electron-shift diagrams provide a good rationale for the fact that, up to **RC**$_{BFCET}$, the doublet and quartet spin states are close in energy (see Tables S1 and S2 in the Supporting Information), while during the C−C bond coupling, the states bifurcate with a great preference for the doublet spin process, as outlined in Figure 7.

***Scheme 6.*** Orbital Occupancy Changes during the C−C Bond Formation Initiated from $^{4,2}$**RC**$_{BFCET}$

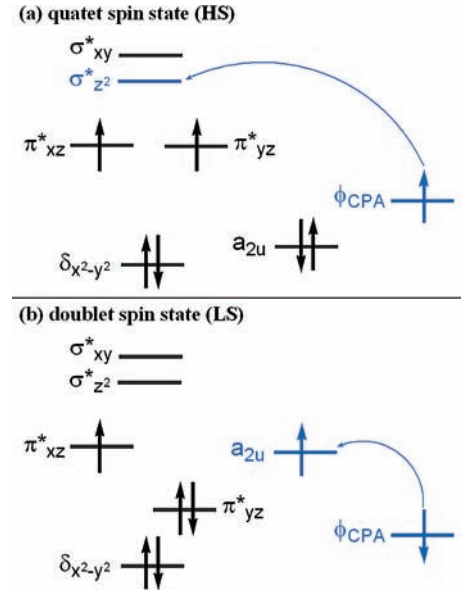


Figure 7a shows that at the UB3LYP(B2//B1):MM level, the transition states on the quartet surface, $^4$**TS**$_{BFCET}$, lie ca. 5.6 kcal/mol higher than the corresponding doublet state species, $^2$**TS**$_{BFCET}$, and, likewise, the C−C bonded LS intermediate $^2$**PC**$_{BFCET}$ is 8.4 kcal/mol more stable than $^4$**PC**$_{BFCET}$. Figure 7b shows the key geometries of the $^{2(4)}$**TS**$_{BFCET}$, which are in line with these relative energies and with the electron-shift diagrams in Scheme 6. As expected from the electron shifts, the largest difference between the two states is concentrated in the heme moiety. Thus, because the quartet state involves an electron shift to the $\sigma^*_{z^2}$ orbital, while in the doublet state the shift occurs to the $a_{2u}$ orbital, the corresponding Fe−OH and Fe−S bonds of the quartet $^4$**TS**$_{BFCET}$ species are longer than those on the doublet $^2$**TS**$_{BFCET}$ state (Fe−OH 1.92 Å and Fe−S 2.68 Å on the HS state, vis-à-vis Fe−OH 1.86 Å and Fe−S 2.44 Å on the LS state). These differences in the bond elongation are responsible for the higher barrier as well as the higher energy of the product cluster, $^4$**PC**$_{BFCET}$, for the quartet state process. Thus, the electron-transfer aspect of the BFCET step is responsible for the spin-state selectivity of the BFCET step. Also, as already noted, these are the water molecules that lower the barrier for this process.

**Subsequent Steps (s6−s10).** Referring back to Scheme 4 and Figure 5, after the BFCET step, the proximal indolic N−H should transfer the proton to the PorFe(III)OH species in $^2$**PC**$_{BFCET}$ (**8**, Scheme 4) to form the ferric−aqua complex **10**. However, in $^2$**PC**$_{BFCET}$, the distance between two proton-transfer terminals is 5.73 Å (Figure S8). Here again, the water molecules come to the rescue in the second water-relocation step (**s5**) followed by PT2 (**s6**) from proximal indole to the heme moiety.

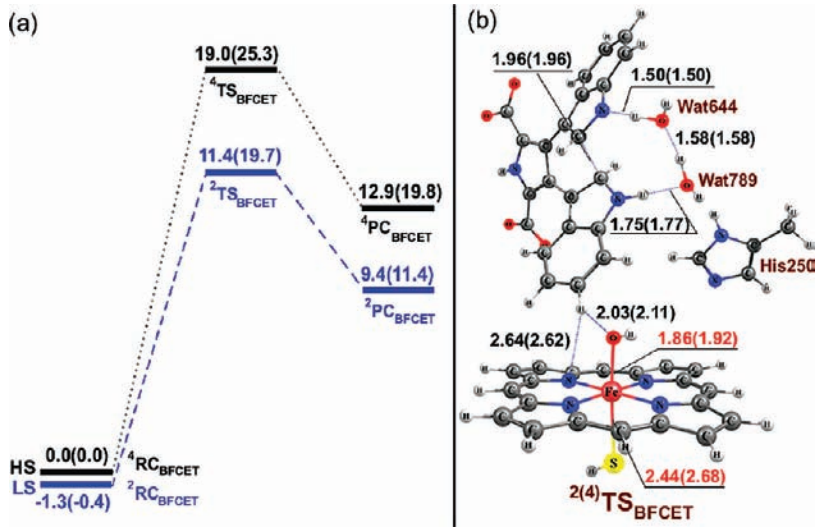


***Figure 7.*** The BFCET step and its spin-state selectivity: (a) The UB3LYP:MM energy profiles (in kcal/mol) for the doublet and quartet states of the C−C bond formation step calculated with the B1(B2) basis sets, respectively. (b) UB3LYP/B1:MM calculated key geometric details of the corresponding transition states $^{2(4)}$**TS**$_{BFCET}$. Lengths are in angstroms.

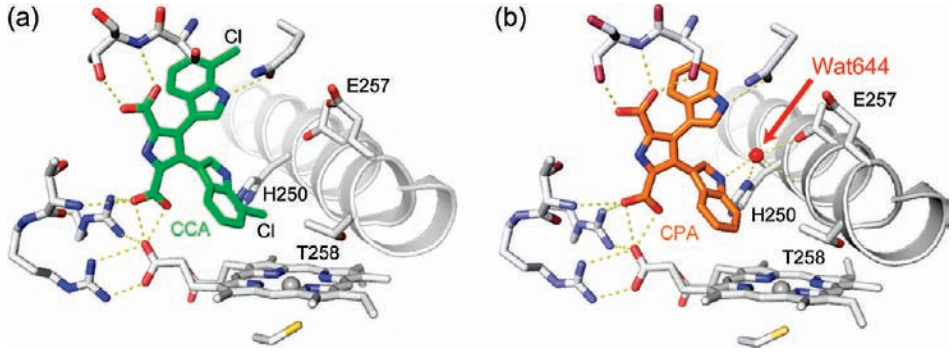


***Figure 8.*** Structural differences between the (a) StaP−CCA and (b) StaP−CPA heme pockets in the crystal structures. Note the absence of wat$_{644}$ in StaP−CCA.

The water ligand in **10** is ligated tightly to the iron core, as the Fe−O(H$_2$) distance is only 2.06 Å (Figure S8); thus the low spin doublet state is the ground state. Subsequently, there is another water-relocation process (**s7**) that enables the water diad to assist now the two intramolecular proton migration processes (steps **s8** and **s10**) from the C-5/C-5′ positions to the vacant N-4/N-4′ positions. Direct rearrangements, without the water molecules, require a strained three-membered cyclic transition state, with barriers exceeding 40 kcal/mol (see Figure S9 in the Supporting Information). With the H-bonding interaction generated by the water-relocation step, **s7**, the strong H-bond effect of the newly formed H-bond network allows one water molecule to transfer a proton to one of the vacant N-4/N-4′ positions and generates a hydroxide ion (Figures S10 in the Supporting Information) that facilitates the proton transfer from the C-5/C-5′ position to this anion, thus keeping a low barrier for PT3, as shown in Figure 5. Subsequently, another water-relocation step (**s9**) facilitates the other proton transfer (step **s10**, PT4) to the second indolic N position at a very low barrier.

**D. What Mechanistic Elements Are Essential to the Function of P450 StaP? An Experimental Testing of the Proposed Mechanism.** The above descriptions in Scheme 4 and Figure 5 indicate very clearly that the key players in the mechanism are the water molecules (Wat$_{644}$ and Wat$_{789}$) and the His$_{250}$ residue. The Cpd I species and the CPA$^{2-}$ substrates are immobilized in their respective sites by the protein and can only participate in two electron-transfer events that are coupled to the bond reorganization events that in turn are conducted by the mobile waters in the Wat$_{644}$−His$_{250}$−Wat$_{789}$ triad. To explore the essential key players of the mechanism, we carried out the following experimental tests: (i) we changed the substrate from CPA to CCA (Scheme 2b), which is a (C-11, C-11′)-chloro derivative of CPA (Figure 8), and (ii) the His$_{250}$ was mutated to phenylalanine (H250F) and to alanine (H250A).

**Crystal Structure of the StaP−CCA Complex.** There are no obvious differences in the overall structure of the CCA−StaP complex and the CPA−StaP complex (0.58 Å rmsd). Little structural differences are found around Thr258 and Glu257, which are critical for oxygen activation. Figure 8 depicts the structures of the StaP−CPA and StaP−CCA complexes. Similar hydrogen bonding and aromatic interactions in the StaP−CCA complex make the conformation and the orientation of the bound CCA very similar to CPA in the StaP−CPA complex. The distances of CCA to iron and CCA to the heme plane are 4.8 and 4.5 Å, respectively. The distal indole ring is slightly moved away from the C-terminal end of the F-helix to avoid clashes with the chlorine atom (Figure S11 in the Supporting Information). The most intriguing feature of the structure is associated with Wat$_{644}$. Thus, in the StaP−CPA complex structure, this water molecule was located between the substrate and the I-helix, which makes hydrogen bonds with the proximal indole ring and His$_{250}$ (highlighted in Figure 8). However, in the

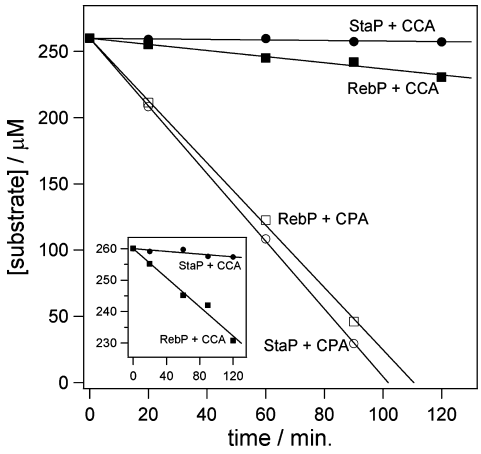


***Figure 9.*** Substrate consumption as a function of time in the reaction of P450 StaP or RebP with CCA or CPA. The inset expands the plots for the reaction with CCA.

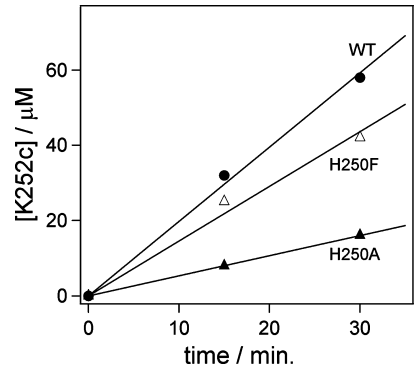


***Figure 10.*** Major product (K252c, Scheme 2) formation, as a function of time, in the reaction of wild-type P450 StaP and its mutants with CPA.

StaP−CCA complex, we could not find any electron density to suggest the presence of a water molecule in the vicinity of CCA.

**Relative Reactivity of StaP toward CCA and CPA.** The crystal structure of the StaP−CCA complex shows that the chlorine atom of the "proximal" indole ring considerably overlaps with a water molecule that will be formed during the formation of StaP Cpd I ($Wat_{789}$), while $Wat_{644}$ near CCA could not be detected. This observation suggests that it should be difficult for StaP to catalyze the deprotonation of CCA in the PCET step (**s1** in Scheme 4).

To test this supposition, we examined the differences in the reactivity of P450 StaP and the analogous RebP enzyme toward CPA versus CCA. Figure 9 depicts the catalytic activity of the two enzymes as rate of depletion in the amounts of the two substrates. It can be seen that the P450 StaP causes a significant consumption of CPA, and a much smaller consumption in the amount of CCA. Similarly, in the presence of P450 RebP, the amounts of CPA decreased as with P450 StaP, whereas the amount of CCA is consumed to a much lesser extent. These results show very clearly that the oxidation of CCA is difficult, be the enzyme StaP or RebP.

The above experimental data are consistent with the crystal structure of the StaP−CCA complex. As shown in Figure 8, CCA takes nearly the same orientation as CPA in the heme pocket. However, while the StaP−CPA structure possesses the crystal water $wat_{644}$, this water molecule is absent in the StaP−CCA crystal structure, which possesses a "dry" heme pocket. Furthermore, the chlorine atom at the C-11 position also blocks the formation of a proton relay pathway, which can connect the substrate to the iron-oxo moiety of the heme, as would be necessary for completion of the PCET step in Scheme 4. This result supports the theoretical conclusion that the proton relay pathway via the $Wat_{644}$−$His_{250}$−$Wat_{789}$ triad is necessary to initiate the oxidation cycle in a PCET step similar to the HRP-catalyzed reaction oxidation of ferulic acid.[4]

**The Activity of the P450 StaP Mutants.** To further identify what is the key element in the proton relay pathway, we carried out site-directed mutation of the $His_{250}$ position and replaced histidine by phenylalanine and alanine. It was reasoned that these mutations would affect the proton-relay triad, because phenylalanine and alanine cannot serve as proton acceptor and donor moieties. The results are shown in Figure 10. It can be seen that the amount of the catalytic product of StaP (K252c in Scheme 2a) decreased to 25% in the presence of H250A mutant as compared to the amount formed in the presence of WT StaP after 30 min. However, with the H250F, the substitution of histidine with phenylalanine is seen from Figure 10 to decrease the amount of K252c to only 72%.

The surprising result with H250F indicates that the histidine residue is not an absolute necessary element in the proton relay pathway. If this indication is correct, there should exist then an alternative proton relay pathway, which utilizes only the $Wat_{644}$−$Wat_{789}$ diad, and which is the minimal necessary mechanism for the function of the enzyme. This hypothesis was tested computationally.

**The Minimally Necessary Water Diad Mechanism.** To test this hypothesis, we performed QM/MM calculations (restricted to UB3LYP/B1) and tested the relative ease of the PCET initiating step (**s1**), using the $Wat_{644}$−$His_{250}$−$Wat_{789}$ triad vis-à-vis the $Wat_{644}$−$Wat_{789}$ diad, in both the wild-type enzymes, and the H250F mutant. The results are shown in Figure 11. It is seen in Figure 11a that in the H250F mutant, the $Wat_{644}$−$Wat_{789}$ diad is indeed an efficient proton relay pathway, exhibiting a barrier of only 7.7 kcal/mol, even lower than the barrier we calculated for the WT enzyme with the $Wat_{644}$−$His_{250}$−$Wat_{789}$ triad (Figure 11b). Therefore, we subsequently explored the feasibility whether the diad mechanism can operate in the WT enzyme too. As can be seen from Figure 11c, the barrier for the diad PCET pathway is now 14.7 kcal/mol, which is 2.7 kcal/mol higher than the corresponding barrier in the triad pathway, in Figure 11b. This is a small difference, but sufficiently large to make the triad path preferred by the WT enzyme, and leaves the diad path for the H250F mutant.

We also explored the difficulty to generate the diad proton relay pathway in the WT enzyme vis-à-vis the H250F mutant. We recall that $Wat_{789}$ is formed along with Cpd I formation. Before the formation of Cpd I and $Wat_{789}$, $Wat_{644}$ must form favorable H-bond connections to stabilize itself in the heme pocket. As shown in the wild-type X-ray structure in Figure 1, $Wat_{644}$ is bound to $His_{250}$ and also with $Thr_{253}$ initially. Subsequently, as shown by the calculations, $Wat_{644}$ moves to $Wat_{789}$ to generate a diad. In the H250F mutant, the calculations show that $Wat_{644}$ is bound only to $Thr_{253}$ initially, because of the mutation at the 250 position, and only then does $Wat_{644}$ move to bind with $Wat_{789}$ (shown in Figure S12 in the Supporting Information) and thereby generate the $Wat_{644}$−$Wat_{789}$ diad. The calculations further show (Figure S12) that the formation of the diad is very easy in the H250F pocket; the calculated UB3LYP(B1):MM barrier is only 0.5 kcal/mol and the $Wat_{644}$ movement is exothermic by 5.4 kcal/mol, while in the WT pocket, the diad formation is less favorable, having a

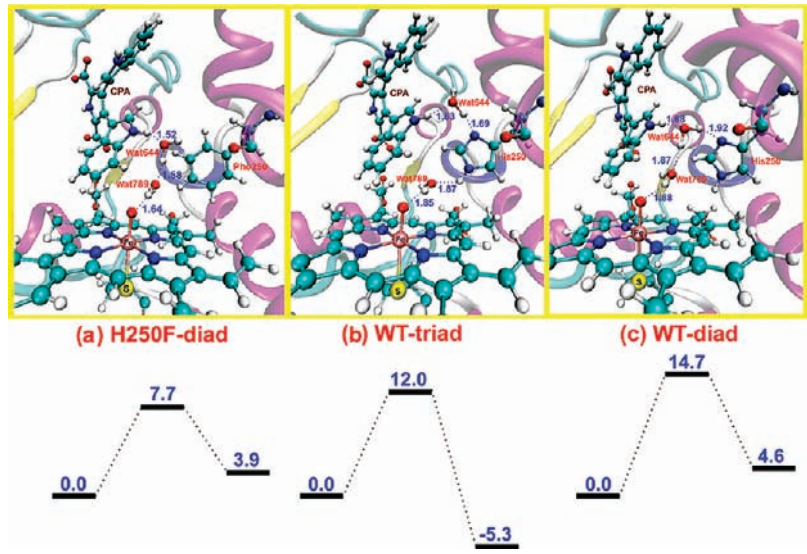


***Figure 11.*** UB3LYP/B1:MM calculated geometries and related energy profiles for the PCET pathways of (a) the $Wat_{644}-Wat_{789}$ diad, and (b) the $Wat_{644}-His_{250}-Wat_{789}$ triad in the WT enzyme and (c) in the H250F mutant.

barrier of 6.7 kcal/mol and the $Wat_{644}$ movement is endothermic by 0.3 kcal/mol. It follows, therefore, that *in the wild-type enzyme, the efficient proton relay pathway is $Wat_{644}-His_{250}-Wat_{789}$ triad, while in the H250F mutant, the proton relay pathway is the $Wat_{644}-Wat_{789}$ diad.* The H250A mutant is different from the H250F, because the replacement of histidine by alanine creates a large space in the heme pocket and will allow for water delocalization rather than clustering to a diad. Therefore, we think that in the H250A, the water diad is floppy and the establishment of the PCET pathway is slower, thus reducing the activity of the H250A mutant significantly.

## Discussion

The ring closure and loss of two H's from CPA by P450 StaP (Scheme 2a) is an intriguing transformation that teaches us about the uncanny solutions found by enzymes to perform its function. Thus, experiment[13] shows that the carboxylic groups of CPA are most likely deprotonated by the enzyme, and the substrate is thereby clawed by the pocket residues, and therefore immobilized quite far from the active species, Cpd I; the Fe−C5/C5′ distance is as large as 8.62 and 10.56 Å, respectively (see Figure S15 in the Supporting Information). Moving the substrate toward Cpd I is costly, and hence CPA remains immobilized away from the active species, and as such no reaction can occur directly between these partners; any reaction must be somehow mediated.[8] Theory shows that the mediation involves three essential elements, which can be gleaned from Scheme 4 and Figures 1, 2, 4, and 5.

The first element derives from the fact that the protein pocket doubly deprotonates CPA to $CPA^{2-}$ and thereby renders it a sufficiently good electron donor to participate in electronic delocalization of the cation radical of the active species. Thus, as suggested originally,[13] by invoking an analogy to C*c*P, theory confirms[8] that Cpd I of P450 StaP is not the usual Cpd I of P450s (see **1** in Scheme 1), but one that involves a cation-radical state that is delocalized over both the porphyrin/sulfur $a_{2u}$ orbital and the indole moiety of CPA. While the extent of delocalization is changing with fluctuation of the enzyme, in any conformation we studied, there is a substantial electron transfer from CPA to Cpd I (see Figure 4), which very easily becomes complete.

This electronic change in CPA activates the substrate and thereby enables it to undergo further changes, and here comes the second and key element: The enzyme pocket involves a proton-shuttle residue, $His_{250}$, and two water molecules, one that exists already in the resting state, $Wat_{644}$, and the other, $Wat_{789}$, that is liberated during the formation of Cpd I by O−O heterolytic cleavage. These moieties form a hydrogen-bonding triad $Wat_{644}-His_{250}-Wat_{789}$ that can shuttle a proton from the N−H group of the immobilized CPA all of the way to the oxo group of Cpd I. During the transfer of this proton along the triad, the electron transfer from CPA to Cpd I becomes complete (Figure 2), so that the net process involves proton-coupled electron transfer (PCET), which sets the entire mechanism in motion (Figure 5).

The third key element is the dynamic ability of the water molecules, $Wat_{644}$ and $Wat_{789}$, to move and mediate all of the rest of the processes, which involve proton transfers and C−C bond formation coupled to a second electron transfer (BFCET) whereby the enzyme comes full cycle (Figures 5 and 7). Even then, the two water molecules do not rest but assist the protons on the carbon atom of C−C closed CPA to migrate to the indolic position. Yet these waters have an even farther-reaching impact on the mechanism as suggested by the combination of experiment and theory.

Thus, experimental tests of the mechanism show that disrupting the water structure has an adverse effect on the function of the enzyme. Changing CPA to the dichloro derivative CCA that kicks off $Wat_{644}$ shows that the enzyme almost loses its function. Mutating $His_{250}$ to Ala, which increases the empty space and will cause water delocalization, lowers the activity of the H250A mutant by 75%. However, it was the H250F mutation that reveals that the two waters are the most important element of the enzyme. Thus, while initially we expected that, due to the role of $His_{250}$, the H250F mutation will be detrimental, the experimental results showed that, in fact, the mutant lost only 30% of it activity as compared to the WT enzyme. Theory then followed and showed that, in this case, $Wat_{644}$ and $Wat_{789}$ form quite easily a well-structured diad (Phe has about the same size as His) that can perform the proton shuttle and mediate the mechanism (Figure 11). Theory further showed that the water-

diad mechanism exists also in the WT enzyme as a secondary mechanism, which is somewhat less favorable than the mechanism of the triad. Thus, *the water diad, $Wat_{644}$ and $Wat_{789}$, is the minimal requisite element to endow the enzyme with function.* It is quite reasonable to assume that the catalysis enabled by the water diad and $His_{250}$ also works for other homologous P450s that are involved in indolocarbazole core biosynthesis (e.g., RebP and AtP[33]) because they are highly homologous to P450 StaP, and especially $His_{250}$ is completely conserved for these P450s.

The critical role of the crystal waters has been suggested before in HRP[34] as means of lowering the barrier for deprotonation of $H_2O_2$ during formation of HRP Cpd I, and recently also as the factor that lowers the barrier for H-abstraction from camphor by P450cam.[15b] Indeed, water molecules are known to be functional in the catalytic cycle of P450,[35] and they play a biological role as biocatalysts.[15] In the present problem, the two waters, $Wat_{644}$ and $Wat_{789}$, are the working class bees of the enzyme, being at all times busy grooming and tending to the needs of the immobilized CPA until it produces its final products. Deciphering this mechanism highlights the importance of the interplay of theory and experiment as an essential kit for tackling complex mechanistic issues as the one treated in the present Article.

## Conclusions

The mechanism of C−C coupling of CPA by P450 StaP, displayed in Scheme 4 and Figure 5, makes a fascinating story, wherein a P450 isozyme replaces its normal mono-oxygenation activity by oxidative aryl−aryl coupling and loss of two protons despite the very large distance between the active species of the enzyme, the high-valent iron-oxo complex called Cpd I, and the substrate, CPA. Thus, using combined theoretical QM/MM calculations and experimental approaches, crystallography, site-directed mutagenesis, and biochemical reactivity assays, it was possible to elucidate a rationale mechanism and interrogate it by experimental means, in a manner enabling us to define the minimal element that endows the enzyme with function.

The combined theoretical and experimental study revealed the following mechanistic features for the wild-type (WT) enzyme: (a) The protein pocket doubly deprotonates CPA to $CPA^{2-}$ and thereby renders it a sufficiently good electron donor to participate in electronic delocalization of the cation radical of Cpd I over both the porphyrin/sulfur $a_{2u}$ orbital and the indole moiety of CPA, such that the complex is a resonance hybrid Cpd I−$CPA^{2-}$ ↔ Cpd II−$CPA^{1-}$, analogous in a way to cytochrome *c* peroxidase,[3,6] as originally proposed,[13] and recently confirmed in a preliminary QM/MM study.[8] Thus, *Cpd I behaves like a chameleon oxidant[5a] and shares its cation radical moiety with the CPA substrate.* (b) This change in CPA activates the substrate and enables it thereby to undergo a proton-coupled electron-transfer (PCET) step, whereby it fully loses the first electron to the heme and also a proton from the proximal indolic N−H moiety. The proton loss is shuttled in a Grotthuss-type mechanism via the hydrogen-bonding triad $Wat_{644}$−$His_{250}$−$Wat_{789}$ that relays the proton to the oxo group of the Cpd I ↔ Cpd II hybrid species. (c) The PCET sets the entire mechanism in motion by means of a C−C bond coupling and four steps of proton transfer and tautomerization, which are all mediated by the water diad $Wat_{644}$−$Wat_{789}$. (d) The C−C formation is coupled by a second electron transfer from CPA to the heme moiety and is hence a bond formation-coupled electron-transfer (BFCET) process; an additional proton transfer regenerates the aqua-ferric resting state and enables the enzyme to come full cycle.

Using the dichlorinated substrate, CCA (Scheme 2), which kicks off $Wat_{644}$, shows that the destruction of the water diad causes a sharp decline in the enzymatic activity. Using the H250F mutant shows by means of experimental reactivity determination and QM/MM calculations that $His_{250}$, while important in the WT enzyme, is not absolutely essential because the water diad $Wat_{644}$−$Wat_{789}$ can carry out the catalysis, albeit less efficiency (75%) than the WT. Thus, the water diad $Wat_{644}$ and $Wat_{789}$ is the minimal requisite element to endow the enzyme with function. These water molecules act, in fact, as biological catalysts, much as found previously in P450cam[15] and in HRP.[34] This study suggests further exploration of the role of the water molecules by experimental means.

**Acknowledgment.** S.S. is supported in part by an Israel Science Foundation (ISF) grant (16/06) and a DIP grant (DIP-G7.1). Y.W. is partially supported by the Lady Davis Fellowship Trust. H.C. thanks the Golda Meir fellowship fund. H.O. is supported in parts by an Industrial Technology Research Grant in 2008 from the New Energy and Industrial Technology Development Organization (NEDO) of Japan. The crystallographic work in this study is supported by grants-in-aid from the Ministry of Education, Culture, Sport, Science and Technology of Japan (to S.N.). This Article is in memoriam of Andreas Fiedler who passed away untimely.

**Supporting Information Available:** Additional 16 figures, 10 tables, and Cartesian coordinates. Complete refs 18a and 22. This material is available free of charge via the Internet at http://pubs.acs.org.

JA9003365

(33) Gao, Q. J.; Zhang, C. S.; Blanchard, S.; Thorson, J. S. *Chem. Biol.* **2006**, *13*, 733–743.
(34) Derat, E.; Shaik, S.; Rovira, C.; Vidossich, P.; Alfonso-Prieto, M. *J. Am. Chem. Soc.* **2007**, *129*, 6346–6347.
(35) Denisov, I. G.; Makris, T. M.; Sligar, S. G.; Schlichting, I. *Chem. Rev.* **2005**, *105*, 2253–2277.